

# Searching Mass-Balance Analysis to Find the Composition of Martian Blueberries

Rif Miles Olsen<sup>1</sup>

<sup>1</sup>Two Planet Life

November 23, 2022

## Abstract

Searching mass-balance analysis is applied to find possible standard oxide composition distributions of Martian blueberries (hematite-rich spherules). This found three groups of complete solution sets to the mass-balance equations consistent with the non-detection of silicates in blueberries (by NASA's rover Opportunity). Two of these groups were previously unknown. One of the groups has blueberry (standard oxide) distributions nearly identical to one found in 2006, with 99.7 wt% FeO/Fe<sub>2</sub>O<sub>3</sub>, 0.3 wt% Ni, and zero content for other oxides. Two of ten investigations found a very small group with composition intermediate to the others. The largest group of 152, 501 complete solution sets have blueberry distributions with average iron oxide content of 91.2 (+/-2.9) wt% and Ni content of 0.30 (+/-0.06) wt%. The main distinguishing feature between the groups is that the blueberry distributions of the largest group have five oxides/elements (MgO, P<sub>2</sub>O<sub>5</sub>, Na<sub>2</sub>O, SO<sub>3</sub>, and Cl) with a collective, summed weight percentage that averages 6.7 (+/- 2.2) wt%. This result is robust to changes in an SiO<sub>2</sub> cut-off that determines inclusion/exclusion in the larger group. Searches over spaces of filtering distributions of basaltic and dusty soils were a methodological advance. The results significantly narrow the possible range of iron oxide weight percentage in blueberries from the conclusions of previous major papers concerned with blueberry composition. The allowed levels of iron oxide are so high, and top, loose blueberries are so plentiful, that blueberries are an attractive source material to start the construction of steel infrastructure for science on Mars.

# Searching Mass-Balance Analysis to Find the Composition of Martian Blueberries

R. M. Olsen<sup>1</sup>

<sup>1</sup>Two Planet Life & Two Planet Steel

Corresponding author: Rif Miles Olsen ([rmo@twoplanet.life](mailto:rmo@twoplanet.life))

## Key Points:

- Searching mass-balance analysis is applied to find possible standard oxide composition distributions of Martian blueberries (hematite-rich spherules).
- Two previously unknown groups of possible blueberry composition distributions are found that have zero or low SiO<sub>2</sub> content.
- Allowable compositions need to be consistent with the non-detection of silicates in blueberries by *Opportunity*'s Mini-TES instrument.
- Searching mass-balance analysis searches over spaces of filtering basaltic and dusty soil distributions.

## 17 **Abstract**

18 Searching mass-balance analysis is applied to find possible standard oxide composition  
19 distributions of Martian blueberries (hematite-rich spherules). This found three groups of  
20 complete solution sets to the mass-balance equations consistent with the non-detection of  
21 silicates in blueberries (by NASA's rover *Opportunity*). Two of these groups were previously  
22 unknown. One of the groups has blueberry (standard oxide) distributions nearly identical to one  
23 found in 2006, with 99.7 wt% FeO/Fe<sub>2</sub>O<sub>3</sub>, 0.3 wt% Ni, and zero content for other oxides. Two of  
24 ten investigations found a very small group with composition intermediate to the others. The  
25 largest group of 152,501 complete solution sets have blueberry distributions with average iron  
26 oxide content of 91.2 (± 2.9) wt% and Ni content of 0.30 (± 0.06) wt%. The main distinguishing  
27 feature between the groups is that the blueberry distributions of the largest group have five  
28 oxides/elements (MgO, P<sub>2</sub>O<sub>5</sub>, Na<sub>2</sub>O, SO<sub>3</sub>, and Cl) with a collective, summed weight percentage  
29 that averages 6.7 (± 2.2) wt%. This result is robust to changes in an SiO<sub>2</sub> cut-off that determines  
30 inclusion/exclusion in the larger group. Searches over spaces of filtering distributions of basaltic  
31 and dusty soils were a methodological advance. The results significantly narrow the possible  
32 range of iron oxide weight percentage in blueberries from the conclusions of previous major  
33 papers concerned with blueberry composition. The allowed levels of iron oxide are so high, and  
34 top, loose blueberries are so plentiful, that blueberries are an attractive source material to start  
35 the construction of steel infrastructure for science on Mars.

36

## 37 **Plain Language Summary**

38 The paper analyses data from NASA's *Opportunity* rover to find the composition of Martian  
39 blueberries. These are roughly spherical, small (1–8 mm diameters), and look blue when seen  
40 against the rusty reds of Mars. *Opportunity*'s scientists realized Martian blueberries contain a lot  
41 of an iron oxide called grey hematite within days of discovering them in January 2004. However,  
42 the resolution of how much hematite and what else blueberries contain remained low, even after  
43 years of effort from the *Opportunity* team. There are vast numbers of loose blueberries lying on  
44 top of soils covering a flat plain larger than Lake Superior. A small fraction could be harvested  
45 (picked from the soil) and then converted into steel infrastructure such as science laboratories,  
46 solar concentrators for electricity generation, landing/take-off pads for space-ships, water  
47 liberation equipment, storage tanks (for breathable air, water, rocket propellant, and more), and  
48 even radio telescopes. The analysis found a previously unknown group of likely blueberry  
49 composition distributions (with around 90% hematite content) that is consistent with an  
50 important non-detection of silicate minerals by *Opportunity*'s instruments – this is good for  
51 converting blueberries into science infrastructure on Mars.

## 52 **1 Introduction**

53 NASA chose to land its Mars Exploration Rover (MER) *Opportunity* on the Meridiani Planum  
54 (Christensen & Ruff, 2004; Christensen et al. 2005). This is a plain with an area larger than Lake  
55 Superior that straddles the equator of Mars (Edgett, 1997). In the late 1990s and early 2000s, a  
56 thermal emission spectrometer (TES) orbiting above Mars (in the *Mars Global Surveyor*) found  
57 signals of surface crystalline, grey hematite (Fe<sub>2</sub>O<sub>3</sub>) across the plain (Christensen & Ruff, 2004;  
58 Christensen et al. 2005). Edgett (1997) and this TES hematite data provided evidence for  
59 abundant flowing water in the plain's far past (Edgett & Parker, 1997; Christensen et al., 2000),

60 since hematite only forms in the presence of water. NASA considered the plain an excellent  
61 place to search for signs of life (Christensen et al. 2005).

62 *Opportunity* made a bouncing landing (Braun & Manning, 2007) into Eagle Crater on the  
63 plain in January 2004. The very first image taken by the scientific PanCam (Bell et al., 2003) had  
64 poor exposure, but it showed an expanse of soil spread from the bottom of the 22 meter diameter  
65 crater to the crater's rim and, near the limit of the camera's resolution, the image showed the soil  
66 covered with thousands of small spherules. In the coming sols (Martian days), *Opportunity's*  
67 team found that the small spherules are rich in grey hematite (Klingelhöfer et al., 2004; *see also*  
68 Bell et al., 2004; Christensen et al., 2004; Rieder et al., 2004), and, when seen against rusty-red  
69 soils, that they look blue. The team quickly called them blueberries.

70 *Opportunity's* PanCam directly imaged huge numbers of blueberries during the rover's  
71 years-long traverse from Eagle Crater to Endeavour Crater (Calvin et al., 2009; *see also* Fenton  
72 et al., 2015; Arvidsen et al., 2006; Soderblom et al., 2004; Squyres et al., 2004). It was soon  
73 realized that loose blueberries on top of soil were probably responsible for the regional-scale  
74 (>150,000 km<sup>2</sup>) surface hematite detection made earlier by the orbiting TES (Squyres et al.,  
75 2004).

76 A recent paper introduced an idea to harvest blueberries with robotic harvesters (Olsen,  
77 2021a). The point of such harvesting is to convert a small fraction of the blueberries into sheet  
78 steel and steel powder, then robotically construct steel infrastructure to support science on and  
79 from the plain (Olsen, 2021a). One subject omitted from that paper is the detailed composition of  
80 hematite-rich blueberries. This subject is, of course, of practical importance to iron- and steel-  
81 making on the plain and is still under-resolved, even after years of efforts by *Opportunity's* team  
82 of scientists. The current paper takes steps toward resolving the composition of blueberries to an  
83 extent necessary for carrying out steel-making in support of science on the Meridiani Planum.

84 This paper is a data analysis paper. The data analyzed comes from public domain  
85 databases; particularly important here is *Opportunity's* alpha-particle x-ray spectrometer (APXS)  
86 oxide abundance (weight percentage) database (Mars Exploration Rover APXS Team, 2016).  
87 The paper will:

- 88 1. Review the instruments that measured blueberries, in particular, what the  
89 instruments actually measured. Review the literature on blueberry composition,  
90 including the literature on mass-balance analysis applied to blueberry data, and,  
91 also, on experiments that add important constraints to blueberry mass-balance  
92 analysis (section 2).
- 93 2. Describe the choice of input APXS data used here (*i.e.*, from among the entire  
94 APXS database) (section 3).
- 95 3. Describe the demixing problem of inferring blueberry compositions from mixed  
96 signals from mixed materials. Introduce spaces of filtering distributions of basaltic  
97 soil and dusty soil compositions. (section 4).
- 98 4. Describe the searching mass-balance analysis procedure (section 5).
- 99 5. Present results from the searches (section 6).
- 100 6. Discuss these results, state conclusions, and outline milestones for future  
101 blueberry composition studies (section 7).

102

103

104

## 105 2 Background

### 106 107 2.1 *Opportunity's* Instruments:

108 *Opportunity's* Athena suite of scientific instruments (Squyres et al, 2003) included  
109 several that could collect data useful for determining the composition of blueberries. The most  
110 focused for composition determinations were a Mössbauer spectrometer (Klingelhöfer et al.,  
111 2003) and an APXS (Rieder, 2003). However, *Opportunity's* Mini-TES (Christensen et al.,  
112 2003), Microscopic Imager (MI) (Herkenhoff et al., 2003), PanCam (Bell et al., 2007), and even  
113 its rock abrasion tool (Gorevan, et al., 2003) all contributed data relevant to the composition of  
114 blueberries.

115 The Mössbauer spectrometer collected data on the abundances of minerals containing  
116 iron, while the APXS instrument collected data on the abundances of 16 elements commonly  
117 found in rocks, soils, and dust. Although, APXS abundances are reported as standard oxide  
118 abundances rather than as elemental abundances (Rieder et al., 2003). Important papers reporting  
119 the collection of APXS and Mössbauer data include Squyres et al. (2004), Reider et al. (2004),  
120 Klingelhöfer et al. (2004), Morris et al. (2006), and Gellert et al. in (2006). Klingelhöfer et al.  
121 (2004) reported the well-known, early “berry bowl” Mössbauer spectrometer experiment that  
122 showed hematite dominates the iron-containing minerals in blueberries.

123 *Opportunity's* MI made many images of interior sections of blueberries (both freshly cut  
124 by the rock abrasion tool and in blueberry fragments). These sections consistently showed that  
125 blueberries have homogeneous interiors without features resolvable at the MI's 30-32 per pixel  
126 resolution (Squyres et al., 2004). This homogeneity makes it possible to extrapolate APXS and  
127 Mössbauer surface results to whole blueberries.

### 128 129 2.2 Data Collection Techniques, Mixed Signals

130 The Mössbauer spectrometer and the APXS were used with similar surface data  
131 collection techniques; that is, each instrument was positioned at a fixed distance from the surface  
132 of target materials to be measured (using a robot arm and surface contact plates), then the  
133 instruments emitted radiation onto the targets, and simultaneously sensed, measured, and  
134 recorded back-radiation.

135 The input data to a blueberry composition analysis (from either the Mössbauer  
136 spectrometer or the APXS) are *mixed signal data from multiple materials*. There are two points  
137 to make about how and why this is so. The first is that the fields of view of both instruments  
138 were large relative to the view area of a single blueberry, even a large one (Squyres et al., 2004;  
139 *see also* Klingelhöfer et al., 2003; Reider et al., 2003). So the composition signals from  
140 blueberries were mixed with those from laterally adjacent materials (Squyres et al., 2004). The  
141 second is that all surface materials on Mars are covered by layers of dust and the thicknesses of  
142 these layers are not negligible relative to the sampling depth of the Mössbauer spectrometer and  
143 the APXS (Morris et al, 2006; *see also* Jolliff, 2005). Thus, since *Opportunity* had no means to  
144 clean the dust off collections of loose blueberries, blueberry composition signals were also mixed  
145 with dust signals (Jolliff, 2005; Jolliff et al., 2007a; Jolliff et al., 2007b; Morris et al, 2006).  
146 Further, although the sampling depth of the Mössbauer spectrometer was shallow (0.2–3 mm  
147 [30, 19]), that of the APXS was shallower (0.02 mm [25]); Morris et. al. (2006) emphasized that  
148 the two instruments sensed significantly different material mixtures, even when placed over the  
149 same sample targets.

150  
151

### 2.3 Experimental Results to Add Constraints to Mass-Balance Analysis

The demixing reported here uses mass-balance analysis applied to APXS data (and possibly in a sequel paper to Mössbauer spectrometer data). A necessary, integral part of any mass-balance analysis are computations using constraint equations, constraint bounds, and constraint sums. However, such mathematical constraints are never enough with mixed material signals. Additional constraints are needed. These should be based either on experimental data, or, at least, some plausible argument or theory. The present balance analysis uses extra experimental data, which is now introduced.

*Opportunity's* Mini-TES instrument and PanCam made measurements that indicate that blueberries have high levels of crystalline hematite (Bell et al., 2004; Calvin et al., 2009; Christensen et al., 2004). These results are not specific enough to draw highly resolved hematite fractions in blueberries, however, any APXS data demixing should find high levels of iron oxide content, and any Mössbauer data demixing should find high levels of hematite.

*Opportunity's* Mini-TES instrument made even more important measurements for strongly restricting possible compositions of blueberries; that is, this Mini-TES could *not* detect silicate minerals above its detection threshold (Calvin et al., 2009). This null result imposes an upper bound on the size of the SiO<sub>2</sub> fraction in APXS blueberry compositions.

Features of basalt and spherule analog composition (in Mars meteorites landed on Earth, in native Earth basalts, and Mars analogs on Hawaii) (Morris et al., 2005; *see also* Dunham et al., 2019; Pang et al., 2008; Tirsch et al., 2012) are reflected in the initial mass-balance results reported below. These features were used in an indirect way in the searching mass-balance analysis to infer the composition of blueberries. In particular, these searches were influenced by Morris et al. (2006) (more in section 5).

### 2.4 Early Blueberry Composition Mass-Balance Analysis

Jolliff (2005) was the first to perform mass-balance analysis on material mixtures to determine the composition of blueberries. He was followed by Morris et al. (2006), and Jolliff et al. (2007b) made another short analysis.

Morris et al. (2006) only considered cases in which the blueberry-containing mixed-materials contained just three component materials: blueberry material, basaltic soil, and dust. This is sensible, as (A) *Opportunity's* sample targeting focused on these cases, and (B) considering blueberry mixtures containing four or more component materials (such as blueberries, basaltic soil, dust, and sediment rock) complicates the analysis. In Jolliff's first, short 2005 discussion of blueberry demixing, he considered mass-balance analysis on a three-component mixture of blueberry material, basaltic soil, and rock, he also mentioned this did not account for the effect of dust. The principal mass-balance equation for analyzing mixtures of blueberry material, basaltic soil, and dust is as follows:

$$\text{Equation (1): } p_k^M = m^{bb} p_k^{bb} + m^{bs} p_k^{bs} + m^D p_k^D, \quad \text{for all } k,$$

In the above equation  $p_k^M$ ,  $p_k^{bb}$ ,  $p_k^{bs}$ , and  $p_k^D$  are weight percentages (or, alternatively, weight or mass fractions) for the material mixture ( $M$ ), the blueberry material ( $bb$ ) (either whole blueberries and/or blueberry fragments), the basaltic soil ( $bs$ ), and the dust ( $D$ ); while  $m^{bb}$ ,  $m^{bs}$ , and  $m^D$  are mixing fractions (which sum to 1) for the blueberry material, the basaltic soil, and the dust. Further, in Equation (1), the subscript index  $k$  that appears in the weight percentages (such as  $p_k^{bb}$ ) is an index indicating either a chemical species (for example, SiO<sub>2</sub>) in APXS data, or a iron-

198 containing mineral (for example, olivine) in Mössbauer spectrometer data. Equation (1) is, in  
199 fact, a set of equations, one each for each possible value of the  $k$  index, and these equations need  
200 to be solved simultaneously.

201 Morris et al. (2006) tested an extreme APXS composition for blueberries with 99.7 wt%  
202 FeO/Fe<sub>2</sub>O<sub>3</sub>, 0.3 wt% Ni, and 0 wt% for all the other 14 oxide/elements. That is, this assumed  
203 blueberry composition, plus guessed mixing fractions, and an average mixed-material  
204 composition were plugged into the set of 16 equations of Equation (1) to compute a composition  
205 of mixed basaltic and dusty soils. They then presented a comparison of this computed mixed soil  
206 distribution to an average mixture of basaltic and dusty soils. These two mixed soil distributions  
207 looked very similar to the eye. Morris et al. (2006) had succeeded in showing that mass-balance  
208 analysis of blueberry/basaltic soil/dusty soil mixtures allowed blueberry compositions with close  
209 to 100% hematite content. However, in the conclusions of Morris et al. (2006), the iron oxide  
210 content of blueberries was only weakly restricted to a broad range: 24–100 wt %. This is not  
211 unreasonable in that mass-balance analysis can be applied to blueberry/basaltic soil/dusty soil  
212 mixtures using other mixing fractions and small changes to the compositions of filtering  
213 distributions to come up with blueberry compositions with very low iron oxide content.  
214 However, this conclusion of Morris et al. (2006) is far from satisfying. It is important to further  
215 constrain mass-balance analysis of blueberry/basaltic soil/dusty soil mixtures. This paper shows  
216 that, with the additional silicate mineral constraint of Calvin et al. (2009), the iron oxide content  
217 in blueberries can be restricted to a much narrower range than the 24–100 wt % of Morris et al.  
218 (2006).

219 Jolliff et al.'s (2007b) conference abstract on blueberry composition applied Equation (1)  
220 using two pairs of sets (of assumed) mixing fractions. (In two pairs the dusty soil mixing fraction  
221 was set to 0, while in the other pair the basaltic soil mixing fraction was set to 0.) And, in all four  
222 of these mixing fraction cases, it was assumed, with seeming reasonableness, that all the (mixed  
223 material, basaltic soil, and dusty soil) weight percentages were averages across the relevant  
224 APXS data. In the four cases, Jolliff et al. (2007b) computed blueberry weight percentages by  
225 solving Equation (1) after inputting their values on the mixing fractions and averaged weight  
226 percentages in their distributions for the mixed materials, basaltic soil, and dusty soil. Given the  
227 average distributions used, the values of the mixing fractions had been chosen so that small  
228 changes to the non-zero mixing fractions produced blueberry compositions that flipped from  
229 being allowable to dis-allowable (that is, their computations produced some blueberry weight  
230 percentages that were negative – negative weight percentages are not physically possible). Jolliff  
231 et al. (2007b) then stressed these results imposed upper limits of around 60 wt% on the  
232 FeO/Fe<sub>2</sub>O<sub>3</sub> percentages in blueberries. Their upper limit was far below the 99.7% FeO/Fe<sub>2</sub>O<sub>3</sub>  
233 weight percentages of Morris et al. (2006). Further, at their upper limit on iron oxide content,  
234 their computed SiO<sub>2</sub> weight percentages were close to 20 wt% and these SiO<sub>2</sub> weight percentages  
235 are *not* reconcilable with the Mini-TES results on the silicate content of blueberries (Christensen  
236 et al. 2004; Calvin et al., 2009).

237

### 238 **3 Data Preparation**

239

240 The APXS data analyzed in this paper comes from *Opportunity's* oxide abundance  
241 database stored in the file `apxs_oxides_mer1.Opportunity.csv` (Mars Exploration Rover APXS  
242 Team, 2016).

243 Each record in the database file is a composition distribution measured from a sampling  
244 target by the APXS instrument. Only some of the distributions in the APXS database file are

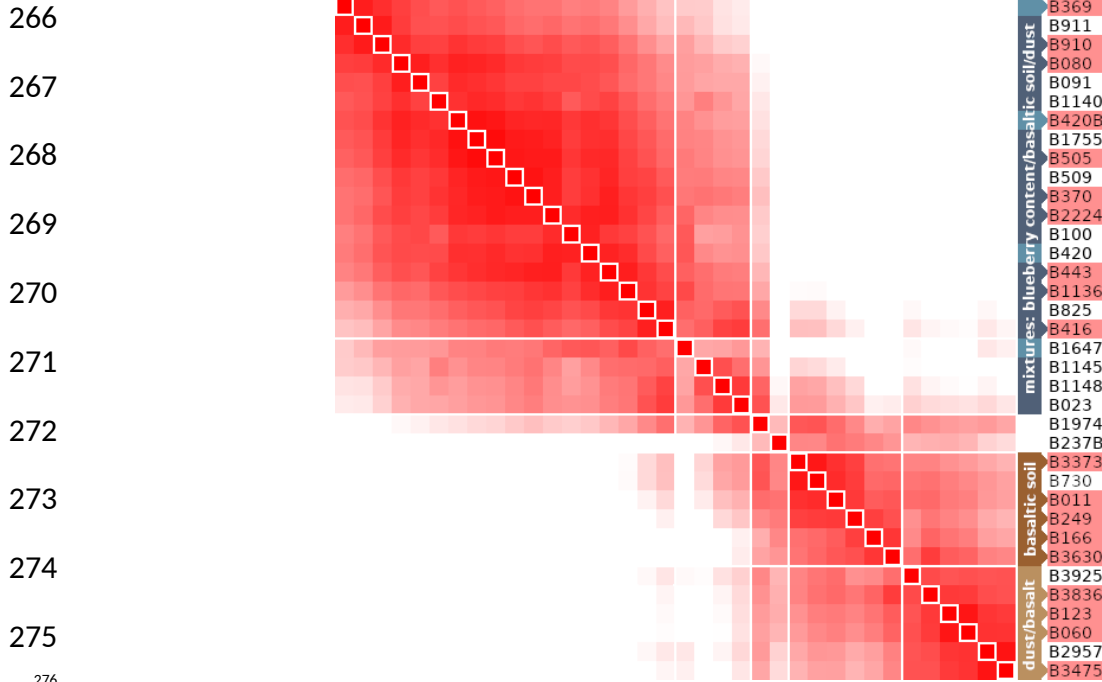
245 used in demixing to determine the compositions of blueberries. The choices of which  
 246 distributions to input to demixing computations were made using: (I) the documentation for the  
 247 database file, (II) a distribution clustering procedure (more below), (III) visual checks of  
 248 *Opportunity's* MI images taken to document the sampling targets from which the APXS took  
 249 distribution measurements, also, (IV) some comments in published papers. Additional details on  
 250 how distributions were chosen is given in an appendix.  
 251

Mixed-Material Distributions (to be demixed)			Basaltic Soil (filtering distributions)		
Database Distribution ID	Shortened Distribution ID	Informal Database Name	Database Distribution ID	Shortened Distribution ID	Informal Database Name
B369_CS	B369	Crest_RippleCrest	B3373_CS	B3373	QueenAdelaide
B910_CS	B910	Marchena	B011_CS	B011	Tarmac
B080_CS	B080	JackRussel_SoilBesi	B249_CS	B249	Rocknest_void_soil
B420B_CS	B420B	RippleCrest_MayNoRooz	B166_CS	B166	Soil_Millstone_Dahlia
B505_CS	B505	Purgatrough_ThroughPlain	B3630_CS	B3630	MulgraveHills
B370_CS	B370	Caviar_undisturbedSoil	<b>Dusty (Top-Layer) Soil (filtering distributions)</b>		
B2224_CS	B2224	OceanWatch	Database Distribution ID	Shortened Distribution ID	Informal Database Name
B443_CS	B443	Recovery_Cure	B3836_CS	B3836	RockCreek
B1136_CS	B1136	Sevilla	B123_CS	B123	HillTop_Wilson
B416_CS	B416	Mobarek_undist_soil	B060_CS	B060	MontBlanc_LeHauches
			B3475_CS	B3475	YGB

252 Table 1: List of Distribution Identifiers. The numbers in these IDs refer to the sol on which the APXS  
 253 measured the target samples.  
 254

255 The list of identifiers of APXS distributions used in demixing is given in Table 1. The  
 256 shortened database IDs will be used here to identify distributions.

257 The distribution clustering to choose distributions proceeded by (A) computing a matrix  
 258 of similarity distances between all pairs of composition distributions for the database's 36  
 259 composition distributions for undisturbed soils, followed by (B) matrix blocking. The blocked  
 260 matrix is in Figure 1, with the pairwise similarity distance values converted to a monochrome  
 261 (red-to-white) scale. The pairwise distances computed for this matrix were Jensen-Shannon  
 262 distances. (Jensen-Shannon distances are used to compare distributions, they are the square roots  
 263 of other distribution similarity measures, called symmetric relative entropies or Jensen-Shannon  
 264 divergences; a readable reference is the Wikipedia page for Jensen-Shannon divergences.)  
 265



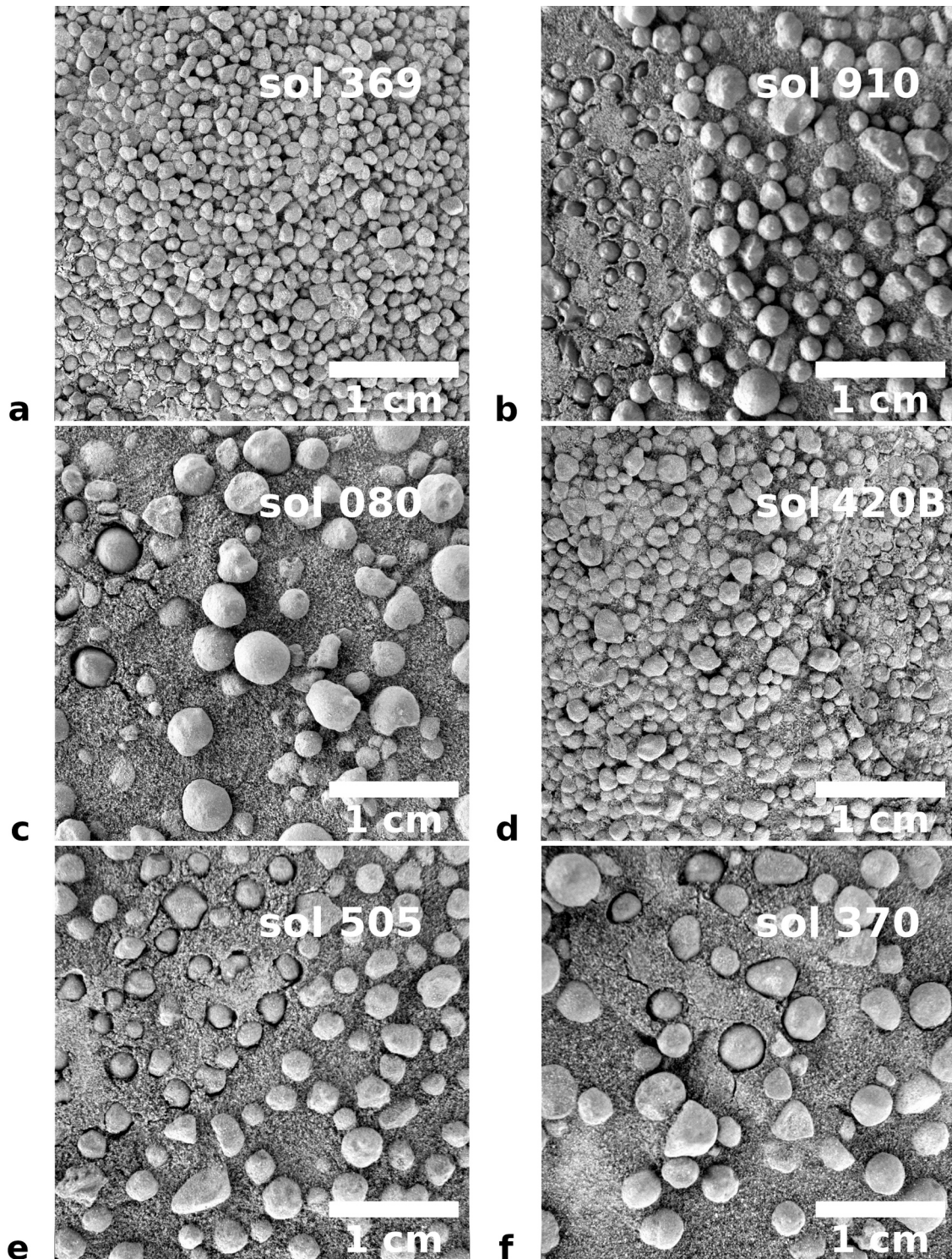
277 Figure 1: Blocked matrix of similarity distances between pairs of distributions.

278  
 279 Relevant images taken by *Opportunity*'s MI are NASA's *Opportunity* Microscopic Imager raw  
 280 image archive (Mars Exploration Rover Microscopic Imager Team, 2016). Figure 2 (covering  
 281 two pages) reproduces the rover's MI images from the mixed material sampling targets with  
 282 distributions chosen for demixing. In addition, Figure 2(k) is an MI image of a basaltic soil that  
 283 was the sampling target for APXS distribution B249, and Figure 2(l) is an MI image of the dusty  
 284 (top-layer) soil that was the sampling target for distribution B3475. *Opportunity*'s MI archive did  
 285 not contain images for all of the basaltic soil and dusty soil APXS sampling targets. Figure 2(k)  
 286 and 2(l) are representative of those basaltic and dusty soil images in the archive.

287 The weight percentages of the chosen mixed material distributions are reproduced (from  
 288 the APXS database) in Table 2 in the order given in the largest matrix block in Figure 1. This  
 289 order makes visible rising and falling weight percentage trends across the table rows, for some of  
 290 the abundant oxides such as CaO, Al<sub>2</sub>O<sub>3</sub>, SiO<sub>2</sub>, and FeO, and also for some of the other  
 291 oxides/elements that will be important for the demixing, including TiO<sub>2</sub>, K<sub>2</sub>O, and Ni, as well as  
 292 the lack of rising/falling trends for some oxide/elements including MgO, P<sub>2</sub>O<sub>5</sub>, Na<sub>2</sub>O, SO<sub>3</sub>, and  
 293 Cl, again these relatively constant weight percentages fractions will be important in demixing.  
 294 Computed Pearson correlation coefficients (not shown) comparing the weight percentages in  
 295 Table 2 for CaO, Al<sub>2</sub>O<sub>3</sub>, SiO<sub>2</sub>, TiO<sub>2</sub>, K<sub>2</sub>O, FeO, and Ni show strong positive correlations between  
 296 the weight percentages of all of CaO, Al<sub>2</sub>O<sub>3</sub>, SiO<sub>2</sub>, TiO<sub>2</sub>, and K<sub>2</sub>O, strong anti-correlations  
 297 between the weight percentages of all of these oxides and those of both FeO and Ni, and a strong  
 298 positive correlation between the weight percentages of FeO and Ni.

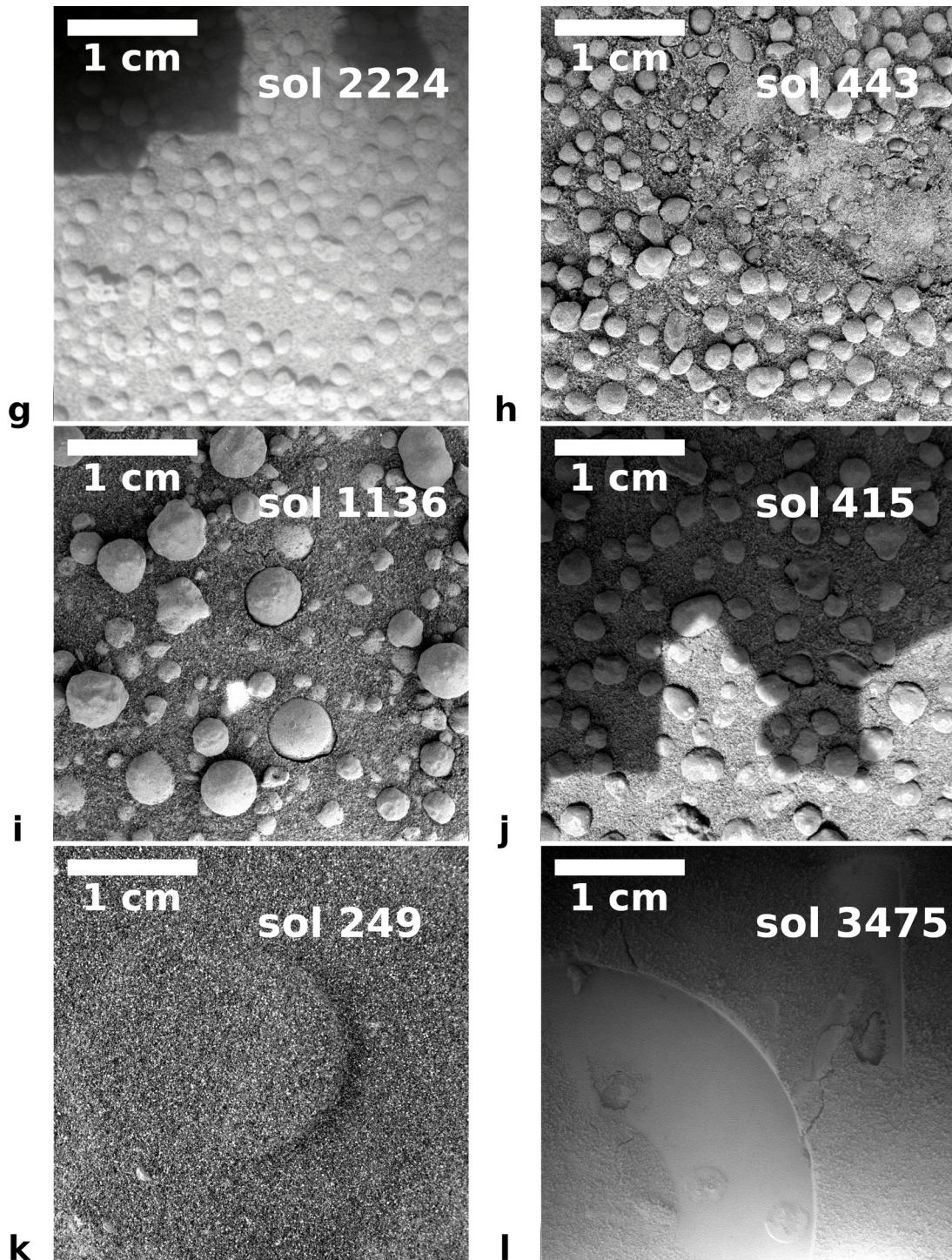
299 Five of the basaltic soil distributions and four of the dusty top-layer distributions were  
 300 chosen (see Figure 1 and Table 1) as filtering distributions in the demixing computations. The  
 301 weight percentages for these filtering distributions are reproduced in Table 3 from the APXS  
 302 oxide abundance database, with the ordering of distributions following that of the second-largest  
 303 matrix block matrix Figure 1.

304  
305  
306  
307  
308  
309  
310  
311  
312  
313  
314  
315  
316  
317  
318  
319  
320  
321  
322  
323  
324  
325



326 Figure 2 (first page): Sampling targets. These are discussed in the text. The order given follows the  
327 distribution order in the largest block in the matrix given in Figure 1. The sol on which each target was  
328 photographed is overlaid. NASA's *Opportunity* archive IDs for these images are (in order):  
329 1M160940202EFF42D9P2956M2M1.JPG, 1M208971634EFF748BP2957M2M1.JPG,  
330 1M135292637EFF10CGP2956M2M1.JPG, 1M165468362EFF5208P2956M2M1.JPG,  
331 1M173018037EFF55VWP2956M2M1.JPG, and 1M161026325EFF42D9P2957M2M1.JPG

332  
 333  
 334  
 335  
 336  
 337  
 338  
 339  
 340  
 341  
 342  
 343  
 344  
 345  
 346  
 347  
 348  
 349  
 350  
 351  
 352



353 Figure 2 (second page): Sampling targets. The order given follows the order in the matrix of Figure 1. The sol  
 354 on which each target was photographed is overlaid. *NOTE, the image given for distribution B416 was actually*  
 355 *taken on sol 415 – the archive had no image that definitely shows the sampling target for distribution B416.*  
 356 NASA's *Opportunity* archive IDs for these images are (in order):  
 357 1M325620114EFFAG00P2939M2M1.JPG, 1M167510573EFF55B0P2956M2M1.JPG,  
 358 1M229031407EFF81D2P2936M2M1.JPG, 1M165026294EFF5200P2956M2M1.JPG,  
 359 1M150287403EFF3620P2976M2M1.JPG, and 1M436679762EFFC9EIP2935M2M1.JPG.

	B369	B910	B080	B420B	B505	B370	B2224	B443	B1136	B416
CaO	4.88	5.04	5.10	5.27	5.39	5.67	5.55	5.69	5.96	6.17
TiO <sub>2</sub>	0.67	0.70	0.68	0.78	0.75	0.78	0.78	0.79	0.82	0.85
K <sub>2</sub> O	0.33	0.36	0.37	0.36	0.39	0.40	0.39	0.43	0.42	0.42
MnO	0.29	0.27	0.27	0.29	0.28	0.29	0.26	0.32	0.29	0.33
Cr <sub>2</sub> O <sub>3</sub>	0.27	0.30	0.30	0.27	0.32	0.32	0.32	0.32	0.31	0.33
Al <sub>2</sub> O <sub>3</sub>	7.36	7.39	7.66	7.76	7.80	7.83	7.78	7.78	7.79	8.19
SiO <sub>2</sub>	37.40	37.90	38.60	39.00	39.30	39.80	39.40	40.00	40.00	41.50
MgO	6.39	6.32	6.81	6.61	6.54	6.61	6.40	6.43	6.62	6.75
P <sub>2</sub> O <sub>5</sub>	0.87	0.82	0.77	0.84	0.82	0.82	0.83	0.83	0.85	0.86
Na <sub>2</sub> O	2.13	2.16	2.21	2.19	2.15	2.17	2.27	2.01	1.96	2.21
SO <sub>3</sub>	4.64	5.28	4.90	5.15	5.24	5.05	5.54	5.54	5.89	5.21
Cl	0.71	0.73	0.68	0.70	0.65	0.68	0.72	0.72	0.75	0.67
Br	0.0101	0.0084	0.0035	0.0096	0.0048	0.0047	0.0055	0.0048	0.0083	0.0039
Zn	0.0357	0.0377	0.0304	0.0348	0.0331	0.0300	0.0332	0.0354	0.0351	0.0282
Ni	0.1292	0.1082	0.0882	0.0965	0.0743	0.0750	0.0716	0.0729	0.0660	0.0608
FeO	33.80	32.50	31.50	30.60	30.20	29.40	29.60	29.00	28.20	26.30
Total	99.9150	99.9243	99.9721	99.9609	99.9422	99.9297	99.9503	99.9731	99.9694	99.8829

360 Table 2 : Weight percentages of 10 distributions measured from mixed-material sample targets.

361

	Basaltic Soil					Dusty (Top Layer) Soil			
	B3373	B011	B249	B166	B3630	B3836	B123	B060	B3475
CaO	7.41	7.31	7.30	7.32	7.52	7.18	6.73	6.59	6.73
TiO <sub>2</sub>	0.95	1.04	0.91	0.85	1.12	1.09	0.97	1.02	1.03
K <sub>2</sub> O	0.45	0.47	0.48	0.55	0.55	0.49	0.51	0.48	0.52
MnO	0.47	0.37	0.40	0.39	0.34	0.34	0.37	0.34	0.36
Cr <sub>2</sub> O <sub>3</sub>	0.48	0.45	0.45	0.34	0.32	0.27	0.36	0.33	0.31
Al <sub>2</sub> O <sub>3</sub>	8.92	9.26	9.59	10.04	9.67	9.51	9.21	9.22	8.79
SiO <sub>2</sub>	45.96	46.30	46.70	47.70	46.73	45.56	45.30	45.30	44.41
MgO	7.29	7.58	7.65	7.14	7.19	7.06	7.61	7.63	7.16
P <sub>2</sub> O <sub>5</sub>	0.81	0.83	0.85	0.81	0.97	1.06	0.87	0.94	1.01
Na <sub>2</sub> O	2.10	1.83	2.39	2.40	2.30	2.21	2.38	2.24	2.25
SO <sub>3</sub>	4.65	4.99	4.62	5.19	5.61	6.53	7.12	7.34	8.07
Cl	0.58	0.63	0.59	0.64	0.78	0.88	0.84	0.79	0.93
Br	0.0023	0.0032	0.0024	0.0025	0.0093	0.0125	0.0035	0.0026	0.0044
Zn	0.0262	0.0241	0.0184	0.0226	0.0226	0.0257	0.0376	0.0404	0.0488
Ni	0.0338	0.0423	0.0344	0.0339	0.0285	0.0282	0.0503	0.0470	0.0482
FeO	19.83	18.80	18.00	16.60	16.79	17.76	17.60	17.60	18.33
Total	99.9673	99.9296	99.9852	100.0290	99.9504	100.0064	99.9614	99.9100	100.0014

362 Table 3: Weight percentages of the distributions measured from basaltic soil and dusty top-layer sample  
363 targets.

## 364 4 Searching Mass-balance Analysis and the Spaces of Basaltic & Dusty Soil Filtering 365 Distributions

366

367 There is variety between the ten mixed-material sampling targets shown in Figure 2 and  
368 between the distributions given in Tables 2 and 3.

369

370 Mass-balance analysis of mixed-material signals to find the composition of one material  
371 (*e.g.*, blueberries) in the mixture is essentially a filtering procedure to subtract (filter) the  
372 potential signals from the mixture's other materials (*e.g.*, basaltic soil and dusty soil) from the  
373 mixed signals (*e.g.*, the data in Table 2) to uncover the composition signal from the material of  
374 interest (blueberries). In the cases investigated, *i.e.*, *Opportunity's* mixed-material sampling  
375 targets, there is no accurate and precise knowledge of the composition of the basaltic and dusty  
376 soils at each sampling site. However, there is information (in Table 3) on the compositions of  
377 basaltic and dusty soils at various other sampling locations. Using averaged basaltic and dusty  
378 soil distributions as filters on the mixed signals failed to find blueberry compositions consistent  
379 with the non-detection of silicate minerals by the Mini-TES instrument. Given this, it makes  
380 sense to search thoroughly with *different*, acceptable pairs of filtering distributions (where one is  
381 a possible basaltic soil distribution, and the other is a possible dusty soil distribution); and, with  
382 each different filtering pair, to subtract signals to find an example blueberry composition. And  
383 repeat this to find many blueberry composition examples that are consistent with the non-  
384 detection of silicate minerals in blueberries. The above is an outline of the searching mass-  
385 balance analysis done to produce the results reported here. The main search is over pairs of  
386 distributions. Section 5 gives more detail. The next thing to do is to describe the spaces of  
387 basaltic and dusty soil distributions.

387

### 388 4.1 Variety and the Spaces of the Filtering (Basaltic Soil and Dust) Distributions

389

390 Each basaltic soil and dust distribution in Table 3 was measured by *Opportunity's* APXS  
391 at specific sampling locations along the rover's traverse across the plain from Eagle Crater then  
392 to and around Endeavour Crater. The physical distances between some pairs of these sampling  
393 locations were over 20 km (for example, the sampling locations for the two basaltic distributions  
394 B3373 and B011). The five basaltic soil distributions given in Table 3 (*i.e.*, B3373, B011, B249,  
395 B166, and B3630) should collectively represent practical guides as to how much variety in  
396 basaltic soil distributions could be measured across the parts of the plain traversed by  
397 *Opportunity*. Similarly, the four dusty soil distributions (*i.e.*, B3836, B123, B060, and B3475)  
398 should collectively represent practical guides to the variety of dusty soil distributions.

399

400 This paper will use these two collections to define spaces of basaltic soil and dusty soil  
401 distributions. The point of these spaces of distributions is to define acceptable basaltic soil and  
402 dusty soil distributions to use as filters in demixing calculations with the mass-balance equations  
403 (Equation (1)). So, for any given distribution used as a filtering basaltic soil distribution, that  
404 distribution must be in the space of basaltic soil distributions. Of course, the extent of the space  
405 of acceptable basaltic soil distributions should be based on the experimentally measured basaltic  
406 soil distributions.

407

408 The space of dusty soil distributions and the space of basaltic soil distributions are both  
409 defined as a central core space plus an extension layer around the core. The central core space of  
410 dusty soil distributions is, for our practical purposes, all those distributions that can be made "in-  
between" the four experimentally measured dusty soil distributions (*i.e.*, B3836, B123, B060,  
and B3475) as linear combinations of these four experimental distributions (with non-negative  
mixing fractions that sum to 1). Similarly, the central core space of basaltic soil distributions is

411 all those distributions that can be made “in-between” the five experimentally measured basaltic  
 412 soil distributions (*i.e.*, B3373, B011, B249, B166, and B3630) as linear combinations these five  
 413 experimental distributions (with non-negative mixing fractions that sum to 1).

414 A helpful analogy for these core spaces is a room. The “room” for the dust core space is a  
 415 tetrahedron with the four experimental distributions (B3836, B123, B060, and B3475) forming  
 416 the room’s “corners,” that is, the tetrahedron’s vertices. Any “in-between” distribution is a point  
 417 inside the room. The distances between any interior point to one of the room’s corners tend to be  
 418 shorter than those from one corner to another. With Jensen-Shannon distance measurement, this  
 419 is also a feature of the interior dusty soil distributions and the “corner” experimental distributions  
 420 (B3836, B123, B060, and B3475). Similar comments hold for the basaltic soil core space defined  
 421 by the five experimental distributions (B3373, B011, B249, B166, and B3630), except now the  
 422 “room’s” shape is a hexahedron with five vertices or corners. Note, the two core “rooms” contain  
 423 the average basaltic soil and dusty soil distributions, these average distributions are at the rooms’  
 424 centers.

425 The practical point about having an extension layer around the cores is that the APXS  
 426 distribution data is incomplete. *Opportunity’s* APXS could have sampled other basaltic soil or  
 427 dusty soil targets and made distribution measurements that fall outside the core spaces. In fact,  
 428 *Opportunity’s* APXS made measurements that *did* exactly this: The dusty soil distribution B3925  
 429 (shown in the blocked distance matrix in Figure 1) is outside the core space for dusty soil  
 430 distributions. By definition, a distribution is considered to be inside the extension layer of the  
 431 basaltic soil space when (a) it is not in the basaltic soil core space, and (b) the distance between  
 432 this distribution and any one of the core space distributions is less than or equal to a maximum  
 433 allowed layer thickness, denoted  $L^T$ , where this distance is measured either as the Jensen-  
 434 Shannon distance or as the norm of the scalar product between the two distributions. The  
 435 definition for the dusty soil case is similar just replace “basaltic soil” with “dusty soil” in the last  
 436 sentence. So, now there is a question of what is a suitable value for  $L^T$ . It is good to use  
 437 *Opportunity’s* actual data, so, for now,  $L^T$  is set equal to the Jensen-Shannon distance between  
 438 the B3925 distribution (outside the dusty soil core) and the measured core dusty soil B3836  
 439 distribution. (Note B3925 is closer to B3836 than the other measured dusty soil distributions,  
 440 B123, B060, and B3475.) However, further analysis of the data might provide reasons to change  
 441 this initial value for  $L^T$ . With this layer thickness value set  $L^T=0.065$ , the B3925 distribution is  
 442 on the boundary of the allowed space of dusty soil distributions.

443

## 444 5 Searching Mass-Balance Computations

445

446 In the searches, for each of the ten mixed-material distributions listed in Table 2, we want  
 447 to demix the mixed-material distributions to find blueberry composition distributions.

448 Ten searching investigations were carried out. Each of these ten investigations was for  
 449 one of the ten mixed-material distributions listed in Table 2. Each single investigation consisted  
 450 of 1,336,608 ( $1,336,608 = 13 \times 126 \times 816$ ) attempts to find a complete solution set to the collection  
 451 of 16 of mass-balance equations (for all of the 16 oxide indices) given by Equation (1). A  
 452 complete solution set consists of (A) a set of three mixing fractions (*i.e.*,  $m^{bb}$ ,  $m^{bs}$ , and  $m^D$  in  
 453 Equation (1)), and (B) three demixed composition distributions (one each for blueberries,  
 454 basaltic soil, and dusty soil) for the 16 APXS oxide/elements. To be a complete solution set, for  
 455 each of the 16 oxide/element cases indexed with  $k$ , the three weight percentages ( $p_k^{bb}$ ,  $p_k^{bs}$ , and  
 456  $p_k^D$ ) from the three composition distributions and their corresponding mixing fractions ( $m^{bb}$ ,  $m^{bs}$ ,

457 and  $m^D$ ) are plugged into the right-hand-side of Equation (1) and precisely compute a value of  
 458 the weight percentage  $p^M_k$  (left-hand-side of Equation (1)) and this computed  $p^M_k$  has to be  
 459 equal the actual  $p^M_k$  from the mixed-material distribution under investigation. (Emphasizing,  
 460 equality between the computed right-hand-side and the actual  $p^M_k$  has to hold for all  $k$  for any  
 461 complete solution set to be valid). The goal of these searching investigations is to find many  
 462 complete solution sets where the weight percentage value of SiO<sub>2</sub> in the blueberry distribution,  
 463  $p^{bb}_{SiO_2}$ , is low and consistent with the non-detection of silicates in blueberries (by *Opportunity's*  
 464 Mini-TES).

465

466 For each of the ten investigations, the following was done:

467

- 468 1. For each of 13 sets of target constraints (more below): A large number (102,816) of input  
 469 pairs of basaltic soil and dusty soil distributions were each individually sent to a  
 470 procedure that varied the basaltic soil distribution and computed a set of the mixing  
 471 fractions (in Equation (1)) and a full set of blueberry weight percentages (collectively a  
 472 blueberry composition distribution).
- 473 2. Each individual variation and computation could fail or succeed at discovering an  
 474 acceptable complete solution set that solved Equation (1) (up to 64-bit computer  
 475 accuracy) for the individual mixed-material distribution under demixing investigation. If  
 476 any one of the 1,336,608 tests/attempts succeeded, then all information for that  
 477 test/attempt was made into a complete solution set record and stored in a database file of  
 478 successful example records of complete solutions sets.

479

480 The 102,816 pairs of initial basaltic soil and dusty soil distributions were all combinations of a  
 481 list of 126 basaltic soil distributions and another list of 816 dusty soil distributions (102,816 =  
 482 126×816). The 126 basaltic soil distributions were part of the core space of basaltic soil  
 483 distributions. Five of these were the “corner” measured distributions (in Table 3), the remaining  
 484 121 were interior distributions in the basaltic core space. Collectively (by construction), these  
 485 126 basaltic soil distributions evenly sampled the basaltic soil core space. Similar construction  
 486 methods were used to make the 816 dusty soil distributions in the core of dusty soil space but  
 487 with a denser sampling. More information on the construction of these distributions is given in  
 488 the README.txt file accompanying the open access database of complete solution sets (found in  
 489 the ten investigations reported on here) that is now in the Zenodo repository (Olsen, 2021b).

490

491 The use of 13 sets of target constraints mentioned in the above outline was motivated by  
 492 Morris et al. (2006). That paper inferred a reasonable combined filtering soil distribution (a  
 493 weighted combination of basaltic soil and dusty soil distributions) by inputting into Equation (1):  
 494 (A) a mixed-material distribution that was made by averaging experimental measurements; and  
 495 (B) a completely specified (made-up) blueberry composition distribution with the FeO/Fe<sub>2</sub>O<sub>3</sub>  
 496 weight percentage set to 99.7 wt%, Ni set percentage set to 0.3% and the weight percentages of  
 497 the fourteen other oxides/elements set to 0%. This method used the authors' experience with  
 498 geology, blueberries, and Hawaiian blueberry analogs (Morris et al., 2005) to assert that many  
 499 APXS oxides were likely to be extremely small or 0%.

499

500 In an effort to both use the idea of constraining some of the oxide/element weight  
 501 percentages to 0% (with is computationally helpful) and also to be more deliberate about how  
 502 many and which oxide/element weight percentages to constrain to 0%, plots of the various oxide  
 weight percentages (found in Table 2) were made against the weight percentages of FeO (also in

503 Table 2). The collection of these plots (not shown) suggested the following ordering of oxides  
 504 most likely to have 0 wt% in blueberries (from most likely to quite possible): CaO & TiO<sub>2</sub>, K<sub>2</sub>O,  
 505 MnO, Cr<sub>2</sub>O<sub>3</sub>, Al<sub>2</sub>O<sub>3</sub>, and SiO<sub>2</sub>. In addition, the weight percentages for bromine (Br) are always so  
 506 low, and had other features (see discussion) that the computations could easily find some basaltic  
 507 soil/dusty soil pairs that could accommodate setting the Br weight percentage to 0% (even with  
 508 Br's mildly positive correlation with FeO). Although Zn also has very low weight percentages  
 509 (see Tables 2 and 3), these are generally higher weight percentages than those of Br, and the Zn  
 510 data does not have the confusing features that Br data has, further Zn is also moderately  
 511 positively correlated to FeO, so it is hard to accommodate a 0 wt% for Zn using fine variations in  
 512 soil compositions. Although MgO is noticeably anti-correlated to both FeO and Ni in mixed  
 513 material distributions, this anti-correlation is not so strong as those between FeO and CaO, TiO<sub>2</sub>,  
 514 K<sub>2</sub>O, Al<sub>2</sub>O<sub>3</sub>, and SiO<sub>2</sub>, while the weight percentages for MgO in mixed materials are high. This  
 515 combination of abundance and only moderately strong anti-correlation generate a question as to  
 516 whether there is or is not any MgO in blueberries. In addition, the weight percentages for all of  
 517 P<sub>2</sub>O<sub>5</sub>, Na<sub>2</sub>O, SO<sub>3</sub>, and Cl in mixed materials are only weakly correlated or anti-correlated with  
 518 those for FeO and Ni, and the weight percentages of these species in mixed material are much  
 519 larger than those of Br, Zn, and Ni. So, for all of P<sub>2</sub>O<sub>5</sub>, Na<sub>2</sub>O, SO<sub>3</sub>, and Cl, there are questions as  
 520 to whether or not these species appear in blueberries. Given the above, the 13 sets of constraints  
 521 used in the initial search program were sequentially constructed to be more and more restrictive.  
 522 The first set constrained the weight percentages of only CaO and TiO<sub>2</sub> to 0 wt%. Continuing with  
 523 addition by one, the seventh set of constraints fixed the weight percentages to 0 wt% for these  
 524 eight oxides/elements: CaO, TiO<sub>2</sub>, K<sub>2</sub>O, MnO, Cr<sub>2</sub>O<sub>3</sub>, Al<sub>2</sub>O<sub>3</sub>, SiO<sub>2</sub>, and Br. The most restrictive  
 525 (thirteenth) set only left FeO and Ni free and enforced 0 wt% on the other fourteen  
 526 oxide/elements.

527 For each input mixed material distribution, the initial program has three levels of  
 528 searching. The two obvious ones are the surveys over (I) the input pairs of soil distributions and  
 529 (II) the list of 13 (0 wt%) constraint sets. The third level of search is through variations to the  
 530 input basaltic soil distribution. These variations are computed in 12×102,816 out of the  
 531 13×102,816 tests run for each mixed material investigation. In the least restrictive constraint set,  
 532 with just two 0 wt% constraints (*i.e.*, those for CaO & TiO<sub>2</sub>), these two constraints can be  
 533 satisfied by adjusting the two free parameters of the three mixing fractions ( $m^{bb}$ ,  $m^{bs}$ ,  $m^D$ ). (That  
 534 is, in this least restrictive case, this adjustment fixes the values of the mixing fractions.) In the  
 535 other 12 cases, the list of constraints cannot be satisfied solely by adjusting the values of the  
 536 mixing fractions. In these cases, the basaltic soil distributions are varied (in addition to the  
 537 mixing fractions) to enforce the longer list of 0 wt% constraints. A least-squares optimization  
 538 procedure (to satisfy the given set of 0 wt% constraints) controls the variations made to the  
 539 basaltic soil distributions.

540 Limitations with this searching procedure are discussed in section 7.

541

## 542 **6 Results**

543 The searches found *three groups* of complete solution sets of Equation (1) that also had  
 544 blueberry SiO<sub>2</sub> weight percentages low enough that the Mini-TES might not have detected any  
 545 silicate minerals. The complete solution sets in the two smaller group are similar to the solution  
 546 set of Morris et al. (2006). These groups of complete solution sets are discussed later.

547 Table 4 presents three examples of complete solution sets from the largest group. These  
 548 solution sets are called ES1 (Example Solution 1), ES2, and ES3. All three sets are complete

Normalized B370 Distribution	Mix Fractions	ES1 (0 wt% SiO <sub>2</sub> solution)			ES2 (approx. 4 wt% SiO <sub>2</sub> solution)			ES3 (approx. 8 wt% SiO <sub>2</sub> solution)		
		Blue- berries	Basaltic Soil VBS_ES1	Dusty Soil	Blue- berries	Basaltic Soil VBS_ES2	Dusty Soil	Blue- berries	Basaltic Soil VBS_ES3	Dusty Soil
		0.131358	0.678260	0.190382	0.154705	0.542889	0.302406	0.169250	0.513955	0.316795
Wt%	oxide/ element	Wt%	Wt%	Wt%	Wt%	Wt%	Wt%	Wt%	Wt%	Wt%
5.673989	CaO	0.000000	6.413284	6.955030	0.000000	6.617250	6.883325	0.000000	6.887379	6.736808
0.780549	TiO <sub>2</sub>	0.000000	0.852454	1.062930	0.000000	0.856116	1.044202	0.000000	0.888499	1.022429
0.400281	K <sub>2</sub> O	0.000000	0.452959	0.488791	0.000000	0.459490	0.498765	0.000000	0.471738	0.498206
0.290204	MnO	0.000000	0.332031	0.341422	0.000000	0.339927	0.349404	0.000000	0.348001	0.351480
0.320225	Cr <sub>2</sub> O <sub>3</sub>	0.000000	0.389953	0.292755	0.000000	0.420106	0.304737	0.000000	0.424085	0.322810
7.835508	Al <sub>2</sub> O <sub>3</sub>	0.000000	8.922918	9.367729	0.000000	9.296128	9.221859	0.000000	9.608095	9.145919
39.827999	SiO <sub>2</sub>	0.000000	45.975034	45.408478	3.991376	47.061342	45.175828	7.985826	47.054104	45.116600
6.614650	MgO	0.772625	7.565293	7.258680	2.800440	7.333427	7.275559	2.056806	7.614304	7.427917
0.820577	P <sub>2</sub> O <sub>5</sub>	0.432700	0.840588	1.016907	0.361378	0.852872	0.997517	0.375598	0.880521	0.961060
2.171527	Na <sub>2</sub> O	2.056408	2.179302	2.223252	1.819080	2.228365	2.249795	1.329206	2.389674	2.267630
5.053553	SO <sub>3</sub>	3.547765	4.825598	6.904612	1.030702	5.013861	7.182825	1.2942830	4.853964	7.385775
0.680478	Cl	0.835382	0.601903	0.853536	0.451194	0.640159	0.870160	0.508903	0.632691	0.849672
0.004703	Br	0.010929	0.002387	0.008660	0.003110	0.003789	0.007160	0.007649	0.003809	0.004581
0.030021	Zn	0.041555	0.027189	0.032151	0.034902	0.025080	0.036395	0.043389	0.019384	0.040137
0.075053	Ni	0.311549	0.040265	0.035813	0.279348	0.036221	0.040250	0.256661	0.033467	0.045494
29.420683	FeO	91.991088	20.578841	17.749252	89.228469	18.815867	17.862220	86.141678	17.890284	17.823481

549 Table 4: Three Example Solutions of Mass-Balance Demixing (Equation (1)) of Mixed-Material Distribution B370.

550

551 solutions sets for the B370 mixed-material distribution (one of the ten distributions listed in  
552 Table 2). These three examples were chosen from many thousands of similar complete solution  
553 sets (more below). These three examples are not better than many other complete solution sets.  
554 They are just examples of complete solution sets with low enough blueberry SiO<sub>2</sub> wt% to be  
555 compatible with the Mini-TES's non-detection of silicate minerals in blueberries. Although ES3  
556 is a borderline case, since its 8 wt% for SiO<sub>2</sub> may be too high for a non-detection of silicate  
557 minerals by *Opportunity's* Mini-TES instrument. (The Mini-TES mineral abundance  
558 measurements were accurate to within 5–10 wt% (Christensen et al., 2003).) The example  
559 solution sets ES2 and ES3 were computed with six oxides (CaO, TiO<sub>2</sub>, K<sub>2</sub>O, MnO, and Cr<sub>2</sub>O<sub>5</sub>,  
560 and Al<sub>2</sub>O<sub>3</sub>) constrained to 0 wt%. ES1 was computed with those six oxides plus SiO<sub>2</sub> constrained  
561 to 0 wt%. The normalized version of distribution B370 (with a total weight percent sum of  
562 exactly 100%) is in the left column of Table 4 to six decimal place accuracy. Similarly, the  
563 mixing fractions and the weight percentages of the three complete solution sets are all given to  
564 six decimal place precision (the full records store at 15 decimal place precision or more). This  
565 precision does *not* imply a high level of certainty in our knowledge of the compositions of  
566 blueberries, basaltic soil, and dust. Rather each complete solution set is just one of many

567 solutions that all solve the mass-balance equations with equally high precision. Collectively, the  
 568 multitude of complete solution sets generate ranges of possible compositions for blueberries,  
 569 basaltic soils, and dusty soils (and the mixing fractions of these). The reason such high precision  
 570 is used in the searches is to find actual solutions to the mass-balance equations (Equations (1)) –  
 571 the calculations to find these solutions are sensitive to small changes.

572 Tables 5(a) and 5(b) give some Jensen-Shannon distances. These provide some  
 573 information on the distances between distributions in the space of basaltic soils, and on the sizes  
 574 of variations between input basaltic soils (to the surveying search) and the varied basaltic soils  
 575 that provide (exact) complete solution sets.

576 Table 5(a) gives a matrix of Jensen-Shannon distances between the five experimentally  
 577 measured basaltic soil distributions in Table 3 and the three Input Basaltic Soil distributions,  
 578 (IBS\_ES1, IBS\_ES2, and IBS\_ES3) to the computations that produced the example solutions  
 579 listed in Table 4. For solution ES1, the input distribution IBS\_ES1 is one the measured  
 580 distributions (B3373), so IBS\_ES1 is not one of the “interior” distributions, but a “corner”  
 581 distribution of the core. For solutions ES2 and ES3, the input distributions IBS\_ES2 and  
 582 IBS\_ES3 are both “interior” distributions. Note, the distances between the two “interior”  
 583 distributions and the corner (measured) distributions are mostly smaller than the distances  
 584 between one measured distribution and another: Table 5(a) gives examples of distances  
 585 consistent with the analogy between a room and the core space of basaltic soil distributions.  
 586

	B3373	B011	B249	B166	B3630	IBS_ES1 = B3373	IBS_ES2	IBS_ES3
B3373	0	0.043	0.056	0.099	0.102	0	0.039	0.062
B011	0.043	0	0.050	0.081	0.077	0.043	0.033	0.049
B249	0.056	0.050	0	0.056	0.071	0.056	0.032	0.015
B166	0.099	0.081	0.056	0	0.048	0.099	0.062	0.046
B3630	0.102	0.077	0.071	0.048	0	0.102	0.065	0.056

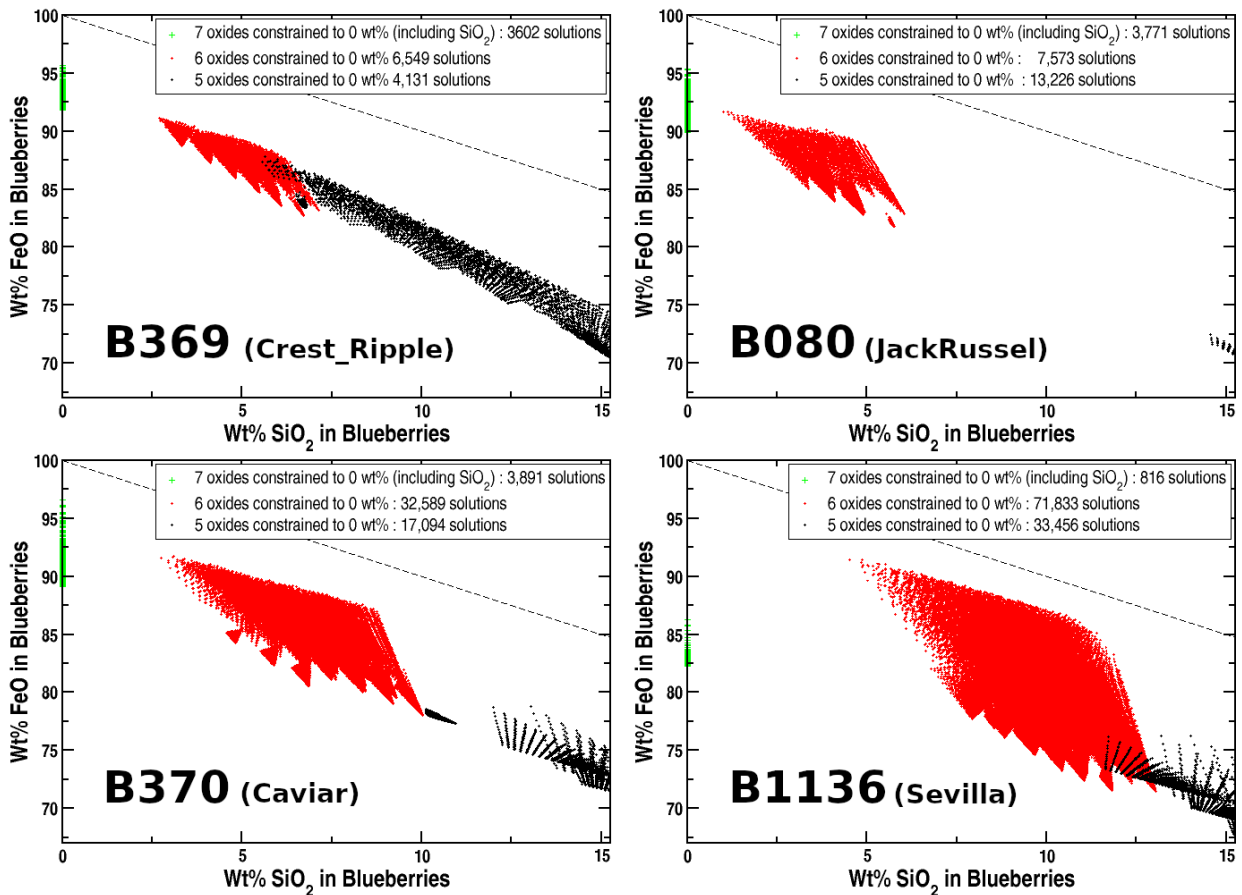
587 Table 5(a): A matrix of Jensen-Shannon Distances between basaltic soil distributions.  
 588

589 Table 5(b) gives Jensen-Shannon distances between the input basaltic soil distributions  
 590 and the final Varied Basaltic Soil distributions (VBS\_ES1, VBS\_ES2, and VBS\_ES3) listed in  
 591 the basaltic soil columns of Table 4. These distances are all smaller than the layer thickness,  
 592  $L_T=0.065$ , defined in section 4.  
 593

Input Basaltic Soil distributions	Varied Basaltic Soil distributions	Jensen-Shannon Distance
IBS_ES1	VBS_ES1	0.052
IBS_ES2	VBS_ES2	0.037
IBS_ES3	VBS_ES3	0.021

594 Table 5b: Jensen-Shannon distances between input basaltic soil distributions and varied basaltic soil  
 595 distributions.  
 596

597 The four scatter plots in Figure 3 present partial information about 189,531 complete  
 598 solution sets where either five, six or seven of the APXS oxides were constrained to 0 wt%.  
 599 These scatter plots use partial information from investigations of four mixed-material  
 600 distributions: B369 (Crest\_Ripple), BO80 (JackRussel), B370 (Caviar) and B1136 (Sevilla).  
 601 These four scatter plots give FeO versus SiO<sub>2</sub> blueberry weight percentages. The legend boxes



602 Figure 3: FeO versus SiO<sub>2</sub> blueberry weight percentage scatter plots.

603

604 give the number of times a complete solution set was successfully computed among 102,816  
 605 computational tests run for each each constraint set, for each mixed-material distribution  
 606 investigated. Complete solutions sets where the previous seven oxides plus Br were constrained  
 607 to 0 wt%, could be used to add more points to the Figure 3 scatter plots, however, these points  
 608 coincided with the points from the seven oxide constraint tests. Scatter plots for the other six  
 609 mixed-material distributions (*i.e.* B910, B420B, B505, B2214, B443, and B416) were similar to  
 610 those shown in Figure 3.

611 An important point to realize about the scatter plots in Figure 3 is that they are rather  
 612 misleading. They are misleading in that they are not showing '+'s at all the locations where they  
 613 could be placed. More complete scatter plots would be thick linear bands with the green, red and  
 614 black "blobs" joined together. The gaps seen between the "blobs" in Figure 3 are artifacts of the  
 615 details of the initial searching mass-balance analysis procedure. This point is returned to in the  
 616 discussion.

617 The Figure 3 scatter plots only reach SiO<sub>2</sub> weight percentages of 15 wt%. However, there  
 618 were other complete set solutions with higher SiO<sub>2</sub> weight percentages and lower FeO weight  
 619 percentages. These solution sets, with higher blueberry SiO<sub>2</sub> content, were computed using  
 620 constraint sets where either two, three, four, or (sometimes) five of the oxides were constrained  
 621 to 0 wt%. These higher blueberry SiO<sub>2</sub> content complete solutions sets are *not* consistent with the  
 622 Mini-TES instrument's non-detection of silicate minerals in blueberries.

623 In the scatter plots of Figure 3, the vertical distance between each point in a scatter plot  
 624 and the dashed diagonal line gives the total weight percentage in blueberries for all the other  
 625 oxide/element species that had more than zero weight percentage and were not FeO or SiO<sub>2</sub>.

626 For the rest of the results on the largest group of complete solutions of the mass-balance  
 627 equations (Equation (1)), three upper cut-offs in SiO<sub>2</sub> content (*i.e.*, 8 wt%, 4 wt%, and 0 wt%)  
 628 are adopted for such solutions to be considered consistent with the non-detection of silicate  
 629 minerals by the Mini-TES instrument. These three cut-offs give alternative operational divides  
 630 for inclusion in the larger group of complete solutions. At least one cut-off value is needed and it  
 631 is not very clear what an optimal cut-off value is. However, since the main new result does not  
 632 change much between the three reasonable cut-off values, the new result is robust to reasonable  
 633 changes in the cut-off value.

634 Table 6 presents averaged blueberry composition weight percentages across the largest  
 635 group of complete solution sets, across the three versions of the largest group defined by the  
 636 upper cut-offs in SiO<sub>2</sub> weight percentage. Each weight percentage row in Table 6 needs a  
 637 separate discussion. The rows for SiO<sub>2</sub> and FeO are discussed immediately. The discussions for  
 638 the other rows are given in the final section.  
 639

	8 wt% SiO <sub>2</sub> cutoff			4 wt% SiO <sub>2</sub> cutoff			0 wt% SiO <sub>2</sub> cutoff		
Number of solutions	311,092			152,501			83,943		
Oxide/element or group	min (wt %)	Ave. ± St.D. (wt %)	max (wt %)	min (wt %)	Ave. ± St.D. (wt %)	max (wt %)	min (wt %)	Ave. ± St.D. (wt %)	max (wt %)
SiO <sub>2</sub>	0.000	3.553 ± 2.616	8.000	0.000	1.254 ± 1.521	4.000	0.000	0.000 ± 0.000	0.000
FeO	77.744	88.661 ± 4.065	98.332	82.252	91.170 ± 2.935	98.322	82.252	93.197 ± 2.318	98.332
Ni	0.185	0.294 ± 0.065	0.520	0.207	0.298 ± 0.062	0.531	0.237	0.322 ± 0.059	0.531
MgO+Na <sub>2</sub> O+P <sub>2</sub> O <sub>5</sub> +SO <sub>3</sub> +Cl	1.296	<b>7.421 ± 2.405</b>	17.365	1.296	<b>6.680 ± 2.222</b>	17.365	1.296	<b>6.414 ± 2.300</b>	17.365
Zn	2×10 <sup>-5</sup>	0.059 ± 0.015	0.101	2×10 <sup>-5</sup>	0.056 ± 0.014	0.101	2×10 <sup>-5</sup>	0.058 ± 0.015	0.101
Br	0.000	0.012 ± 0.011	0.050	0.000	0.009 ± 0.012	0.050	0.000	0.009 ± 0.016	0.050

640 Table 6: Blueberry composition averaged over the larger group of complete solution sets. Averages given to  
 641 two significant digits in Br wt%, and to three decimal places in the others to vertically align numbers.

642  
 643 The averages given for SiO<sub>2</sub> in Table 6 are essentially those of a free parameter that is  
 644 being adjusted by the value of the cutoff value. These values only make sense to the extent that  
 645 the cutoff values make sense. Turning to the FeO numbers in Table 6, the changes in the weight  
 646 percentage averages for FeO are strongly anti-correlated to the changes in those for SiO<sub>2</sub>, so the  
 647 changes to the FeO averages are also driven by the changes in the cutoff value. However, the  
 648 changes in the FeO averages are slightly larger than those in the SiO<sub>2</sub> averages, and, of course,  
 649 the absolute values of all the FeO averages are very high (between 88 and 93 wt%), but not  
 650 extremely close to 100 wt%.

651 Table 7 gives the number of times a complete solution set was successfully computed  
 652 among 102,816 computational tests run, for different constraint set cases, for all the mixed-  
 653 material distributions investigated. Some constraint set cases do not appear in Table 7. In  
 654 particular, the least restrictive cases, with only 2, 3, or 4 of the oxides constrained to have zero  
 655 weight percentage. For these three constraint set cases, there were many thousands of allowable

# oxides constrained to 0 wt%	Constrained Oxides	Mixed-Material Distributions									
	Always constrained: CaO & TiO <sub>2</sub> & K <sub>2</sub> O & MnO	B369	B910	B080	B420B	B505	B370	B2224	B443	B1136	B416
5	Previous & Cr <sub>2</sub> O <sub>3</sub>	4,131	14,688	13,226	22,779	7,344	17,094	0	21,530	33,456	18,108
6	Previous & Al <sub>2</sub> O <sub>3</sub>	6,549	56,737	7,573	5,626	44,917	32,589	61,611	59,706	71,833	12,428
7	Previous & SiO <sub>2</sub>	3,602	816	3,771	8,730	3,606	3,891	807	0	816	1,149
8	Previous & Br	0	0	20,749	0	10,146	10,576	4,197	207	0	10,880
9	Previous & Zn	0	0	0	0	0	0	0	0	0	211
10	Previous & MgO	0	0	0	0	0	0	0	0	0	68
11	Previous & P <sub>2</sub> O <sub>5</sub>	0	0	0	0	0	0	0	11	0	0
12	Everything EXCEPT FeO, Ni, Cl, & SO <sub>3</sub>	0	0	0	0	0	0	0	457	2,989	0
13	Everything EXCEPT FeO, Ni, & Cl	0	0	0	0	0	0	0	12,927	7,444	0
14	Everything EXCEPT FeO & Ni	0 (0)	0 (776)	0 (813)	0 (3,595)	4,765 (45,463)	802 (4,004)	0 (11,724)	88 (11,540)	8 (9,656)	7,915 (17,393)

656 Table 7: Number of allowed solutions to Equation (1) found in sets of 102,816 searches for each of the 10  
657 mixed-material distributions. The numbers in parentheses for the most restrictive constraint set, are the  
658 numbers of complete solution sets that precisely solved Equation (1), but for which the varied basaltic soil  
659 distribution in the solution was not part of the allowed basaltic soil distribution space.  
660

661 complete solutions, however they all had weight percentages for SiO<sub>2</sub> that were not consistent  
662 with the Mini-TES instruments non-detection of silicate minerals. The same is true of almost all  
663 the complete solution sets with 5 of the oxides constrained to have zero weight percentage;  
664 however, a small minority (see Figure 3) of the 4,131 solutions with 5 oxides constrained for the  
665 B369 investigation had SiO<sub>2</sub> weight percentages between 4 wt% and 8 wt% (this small number  
666 of solutions was not used for the statistics counted for the largest group of complete solution  
667 sets).

668 The complete solution sets included in the largest group were all of those with 7 or 8  
669 oxides constrained to 0 wt% (their SiO<sub>2</sub> levels were always 0 wt%) and all those solution sets  
670 with 6 oxides constrained to 0 wt% that also had SiO<sub>2</sub> levels below the cut-offs.

671 In nine of ten investigations zero complete solution sets were found with 9 or 10 oxides  
672 constrained to 0 wt%. The small number (211 + 68) of complete solution sets found in the B416  
673 investigation, with 9 or 10 oxides constrained, had very similar blueberry distributions to those  
674 initially included in the largest group of solutions sets, so these are included in the largest group  
675 of solution sets (although they were not included in the statistics reported in Table 6.)

676 All rows of Table 7 have been discussed except those with 11, 12, 13, or 14 oxides  
677 constrained to 0 wt%. The complete solution sets associated with the last two of these rows have  
678 blueberry distributions that are very similar to expertly forced example solution of Morris et al.  
679 (2006). These solutions associated with the last two rows of Table 7 form the second main  
680 group of complete solution sets that this initial searching mass-balance investigation found.  
681 Table 8 summarizes the blueberry composition results for this second, smaller group.

682

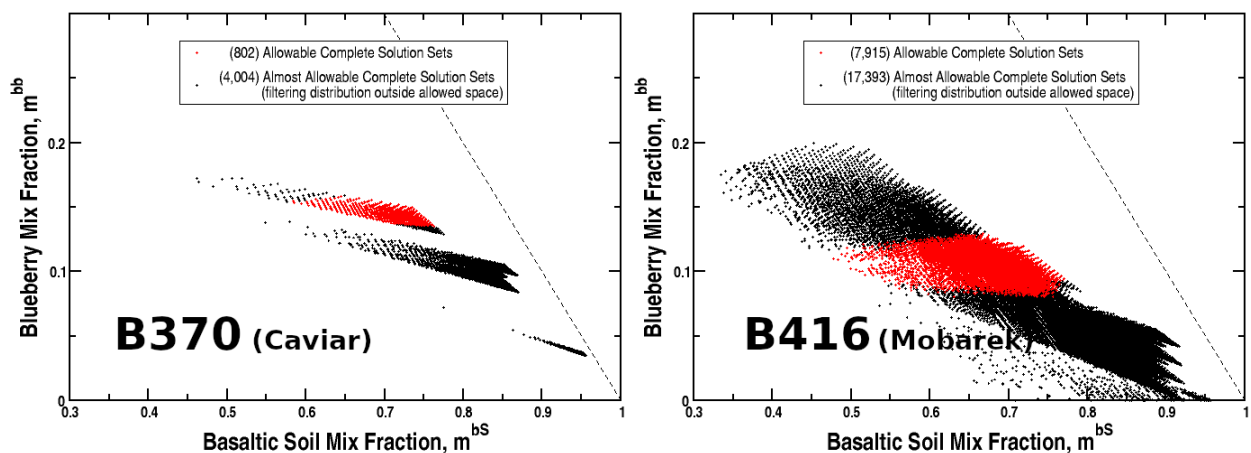
683

# oxides constrained to 0 wt%	Mixed-Material Distributions	# solution sets*	Wt% FeO in blueberries Ave. $\pm$ St.D. (wt %)	Wt% Ni in blueberries Ave. $\pm$ St.D. (wt %)	Wt% Cl in blueberries Ave. $\pm$ St.D. (wt %)
13	B443 & B1136	20,391	99.4506 $\pm$ 0.1277	0.2597 $\pm$ 0.0020	0.2896 $\pm$ 0.1386
14	B505, B370, B443, B1136, & B416	13,578	99.7193 $\pm$ 0.0189	0.2807 $\pm$ 0.0189	0.0000 $\pm$ 0.0000

684 Table 8: Blueberry composition averaged over the second group of complete solution sets (most  
685 restrictive constraint set cases).  
686

687 Only the B433 investigation produced any (just 11) complete solution sets for search  
688 cases with 11 oxides constrained to 0 wt%. These solution sets had blueberry composition  
689 distributions very close (results not shown) to those specified in Table 8 for the second group of  
690 solutions. These eleven solution sets should be grouped with second group of solutions.  
691

692 Scatter plot Figure 4 summarizes the mixing fraction results for the most constrained  
693 computations in the B370 and B416 investigations. Figure 4 highlights a point that is especially  
694 prevalent for the results for the second group of complete solution sets. That is, many complete  
695 solutions sets were found by the searches program that precisely solved the mass-balance  
696 equations (Equation (1)); however, the variation in the input basalt soil distribution produced a  
697 varied distribution that could no longer be considered part of the space of basaltic soil  
698 distributions. Whenever a variation produced this outcome the solution could not be accepted.  
699 The numbers in parenthesis in the last row of Table 7 record how often these cases happened.  
700 The mixing fraction scatter plots in Figure 4 include points for the complete solutions that were  
701 rejected. In each mixing fraction scatter plot there is a clear separation between the accepted and  
702 rejected complete solutions.  
703



704 Figure 4: Mix fractions complete solutions of the smaller group.  
705

706 The ten investigations found one more small group of complete solution sets, where the  
707 SiO<sub>2</sub> content in the set's blueberry distribution is low enough to be consistent with the non-  
708 detection of silicates in blueberries. These solutions sets were found only in the B443 and B1136  
709 investigations with 12 oxides constrained to 0 wt %. The blueberry compositions statistics for  
710 these 3,446 (457+2,989) complete solution sets are given in Table 9.  
711

# oxides constrained to 0 wt%	Mixed-Material Distributions	# solution sets	Wt% FeO in blueberries Ave. $\pm$ St.D. (wt %)	Wt% Ni in blueberries Ave. $\pm$ St.D. (wt %)	Wt% Cl in blueberries Ave. $\pm$ St.D. (wt %)	Wt% SO <sub>3</sub> in blueberries Ave. $\pm$ St.D. (wt %)
12	B443 & B1136	3,446	97.1575 $\pm$ 1.4275	0.2806 $\pm$ 0.0225	0.2674 $\pm$ 0.1123	2.2944 $\pm$ 1.355

712 Table 9: Blueberry composition averaged over the third (smallest) group of complete solution sets.  
713

## 714 7 Discussion and Conclusions

715

716 The search procedure found a large group of complete solutions sets with blueberry  
717 distributions summarized by the results in Table 6. This table outlines possible blueberry  
718 distributions significantly different from those in Table 8, where the Table 8 solutions are very  
719 similar to the asserted blueberry composition of Morris et al. (2006). A third, much smaller,  
720 group of complete solution sets was found with blueberry composition distributions summarized  
721 in Table 9, that are intermediate to those in Tables 6 and 8.

722 The results section discussed the SiO<sub>2</sub> and FeO rows in Table 6. Turning to the Ni row of  
723 Table 6, it is noteworthy that the weight percentages for Ni in Tables 6, 8, and 9 are similar and  
724 close to 0.3 % (just like Morris et al. (2006)). These levels are all enhanced over the Ni levels in  
725 the distributions of Table 2. This is expected, since the Ni levels in Table 2 are, in turn, enhanced  
726 over those in the filtering distributions in Table 3. The row in Table 6 with the most uncertain,  
727 and most undetermined, results is that for Br. The Br data in Tables 3 and 4 forces this  
728 uncertainty. In all distributions given in Tables 3 and 4, the weight percentages for Br are low.  
729 However, there are large relative differences in Br levels between distributions in Table 3. In  
730 particular, distributions B3630 and B3836 have Br levels 3.5–5 times higher than distributions  
731 B249, B166, and B060. Further, although the Br levels in the mixed-material distributions in  
732 Table 2 tend to be higher than those in Table 3, the Br levels in distributions B3630 and B3836  
733 from Table 3 are higher than most of those in Table 2. With these data features for Br, searching  
734 mass-balance calculations that allow Br to have larger than zero weight percentages will find  
735 enhanced levels of Br in blueberries because there are several basaltic and dusty soils (in Table  
736 3) with lower Br levels than those in the mixed material distributions (in Table 2). However, if  
737 solutions are sought in which the Br level is constrained to 0 wt %, then such solutions can also  
738 be found for most of the distributions in Table 2 because the Br levels in B3630 and B3836 are  
739 so high that these can be used as filters that accommodate all the Br in the mixed materials while  
740 holding the blueberry Br content to 0 wt%. The only possible way to improve this situation is to  
741 re-process the relevant raw data to improve the accuracy and precision of the database Br weight  
742 percentages; if this re-processing found Br levels without the large relative differences now  
743 found in Table 3, then a satisfactory Br weight percentage in blueberries could be calculated.

744 The Zn levels in Table 2 are all enhanced over the Zn levels in the basaltic soil  
745 distributions in Table 3, while three of four of the dusty soil distributions in Table 3 have higher  
746 Zn levels than the mixed-material distributions in Table 2. This is an interesting background to  
747 the Zn levels given in the blueberry distributions in Table 6. These average blueberry Zn levels  
748 (in Table 6) are enhanced over all the distributions in both Tables 3 and 4. Given the Zn data in  
749 Tables 3 and 4, this enhancement in average blueberry Zn levels can only occur (and will occur)  
750 if the mixing fraction for the basaltic soil distribution is noticeably bigger than the mixing  
751 fraction of the dusty soil distribution in most of the complete solutions sets (in the largest  
752 solution group from which the Table 6 results are drawn). This does occur in the example  
753 solutions ES1, ES2, and ES3 given in Table 4. However, this extra mixing fraction weight given

753 to basaltic soil distributions relative to dusty soil distributions is not determined by solving the  
754 mass-balance equations for the Zn case; rather, this preponderance for the basaltic mixing  
755 fraction is driven by the mixed-material data in Table 2 for the oxides CaO, TiO<sub>2</sub>, K<sub>2</sub>O, MnO,  
756 Cr<sub>2</sub>O<sub>5</sub>, and Al<sub>2</sub>O<sub>3</sub> (and sometimes SiO<sub>2</sub>) and the least-squares procedure to solve the mass  
757 balance equations that ensure that the weight percentages are zero for these oxides.

758 There is one more row in Table 6 left to discuss, the row for the group of five species  
759 (MgO, Na<sub>2</sub>O, P<sub>2</sub>O<sub>5</sub>, SO<sub>3</sub>, and Cl). The average summed total weight percentages for these five  
760 species is remarkably high (at around 7%) and robust to changes in the cutoff value that  
761 determines which of the complete solution sets are included in the larger group. At the most  
762 conservative cutoff value of zero in the weight percentage of SiO<sub>2</sub> in blueberries, the average  
763 summed total weight percentages for the five species remains high at 6.4 wt%. Note, this most  
764 conservative cutoff of 0 wt% SiO<sub>2</sub> in blueberries corresponds to the *most extreme possible*  
765 *interpretation* of the Mini-TES's non-detection of silicate minerals in blueberries. That is, this 0  
766 wt% SiO<sub>2</sub> in blueberries implies that blueberries contain no silicate minerals at all. So, while  
767 finding 83,943 complete solution sets in the larger group with 0 wt% SiO<sub>2</sub> in the blueberry  
768 distribution, it is an impressively robust result that the average total weight percent for the five  
769 species (MgO, Na<sub>2</sub>O, P<sub>2</sub>O<sub>5</sub>, SO<sub>3</sub>, and Cl) remains between 6 and 7 wt%.

770 In the larger group of complete solution sets, MgO, Na<sub>2</sub>O, P<sub>2</sub>O<sub>5</sub>, SO<sub>3</sub>, and Cl are in  
771 blueberries at well above trace levels. The large number of possible geochemical pathways that  
772 these five species could factor into in blueberry formation processes are significantly different to,  
773 and more flexible than, the geochemistry (and exclusion means) needed to form blueberries with  
774 the severely pure, hematite-and-nickel-only blueberry composition example asserted by Morris  
775 et al. (2006) (with 99.7 wt% FeO/Fe<sub>2</sub>O<sub>3</sub>, 0.3 wt% Ni and 0 wt% for all other oxide/elements).  
776 Geologically plausible blueberry formation histories that are consistent with the averaged  
777 blueberry compositions (in Table 6) of the largest group are likely much easier to posit than  
778 histories leading to the formation of blueberries with the averaged, hematite-and-nickel-only  
779 blueberry compositions (in Table 8) of the second group of complete solution sets.

780 The Hawaiian analogs of blueberries studied by Morris et al. (2005) have composition  
781 features that make them rather more like the blueberry compositions of the new largest group  
782 than the asserted composition of Morris et al. (2006) and the compositions of the second group.  
783 That is, the breccia HWMK745R spherule sample composition reported in Morris et al. (2005)  
784 had FeO/Fe<sub>2</sub>O<sub>3</sub> content at 90.90 wt% (significantly below 99.7 wt%), SiO<sub>2</sub> content at 1.93 wt%  
785 (which is above-zero, but small enough to be below Mini-TES silicate detection), with a balance  
786 of around 7 wt% (although that balance was *not* mainly due to MgO, Na<sub>2</sub>O, P<sub>2</sub>O<sub>5</sub>, SO<sub>3</sub>, and Cl).

787 It is possible that the largest group can be divided into sub-groups based on distinct  
788 composition signatures from among the five species MgO, Na<sub>2</sub>O, P<sub>2</sub>O<sub>5</sub>, SO<sub>3</sub>, and Cl. For  
789 example, comparing blueberry composition distributions in ES1 and ES2 (Table 4), the MgO  
790 content in ES2 is much higher than in ES1, and the SO<sub>3</sub> and Cl content is much higher in ES1  
791 compared to ES2. ES2, with close to 4 wt% SiO<sub>2</sub>, is consistent with some olivine content in  
792 blueberries, ES1 is not, but ES1 is consistent with sulfur mineral content in blueberries.

793 The paper investigated ten different mixed-material distributions. It has not reported on  
794 the differences between the complete solution sets found in the ten investigations. This is partly  
795 due to a desire to avoid overloading the paper with subject matter, and also, in part, due to the  
796 lack of completeness of the initial results (more below). However, here are brief impressions on  
797 blueberry variability: Blueberry compositions across widely spaced sampling locations appear  
798 very similar, but there are small variations.

799 The main conclusions of the paper are: (1) the spaces of basaltic and dusty soil  
800 distributions enabled searching mass-balance analysis to be carried out; (2) that the searching  
801 mass-balance analysis found one large and one small new groups of complete solution sets (of  
802 the mass-balance equations) that are consistent with the non-detection of silicate minerals; (3)  
803 that the averaged blueberry composition associated with the large new group is summarized in  
804 Table 6; (4) that within the new group, SiO<sub>2</sub> content can vary from 0 wt% (which corresponds to  
805 no silicate minerals in blueberries at all) to somewhere around 8 wt% (which corresponds to the  
806 upper limit for consistency with the non-detection of silicates in blueberries) while (on average)  
807 the total content due to the five species MgO, Na<sub>2</sub>O, P<sub>2</sub>O<sub>5</sub>, SO<sub>3</sub>, and Cl remains stable at round 7  
808 wt%; (5) that alterations to the group inclusion/rejection cut-off value for SiO<sub>2</sub> wt% do *not*  
809 change a defining feature of the composition distributions included in the large, new group,  
810 namely the total content due to the five species MgO, Na<sub>2</sub>O, P<sub>2</sub>O<sub>5</sub>, SO<sub>3</sub>, and Cl is well above  
811 trace levels and, on average, is around 7 wt%, so that this feature of the large, new group is  
812 robust to changes in the cut-off value for SiO<sub>2</sub> wt% with changes in the range of 0 wt% to 8 wt%.

813 However, the initial searches did not find many other complete solution sets. And many  
814 of these are easy to specify, given those already found. For example, the linear combination of  
815 the two example solutions ES1 and ES2 in Table 4, with mixing fractions of 0.75 for ES1 and  
816 0.25 for ES2, will produce a new acceptable complete solution set with 1.12 wt% SiO<sub>2</sub> and  
817 91.21 wt% FeO in the set's blueberry distribution: This new solution set fits into the gap between  
818 the red scatter plot and the green scatter plot in Figure 4 for the B370 distribution. Indeed the  
819 whole gap between these red and green scatter plots can be filled with various linear  
820 combinations of pairs of complete solutions sets associated with the red and green scatter plots.  
821 And, of course, the same can be done for the other mixed-material distributions.

822 The initial searches found the largest group of complete solution sets by finding many  
823 examples in it. This is a good start. However, stronger search results are needed to find the holy  
824 grail of blueberry composition studies, that is, to find an accurate range of all possible blueberry  
825 compositions while minimizing this range to the greatest extent the data allows.

826 The quest for this holy grail will reach milestones if any of the following occur: (a) all  
827 groups of complete solution sets consistent with the non-detection of silicates are found; (b) it is  
828 demonstrated that all of these groups are found; (c) the full range or extent of any of these groups  
829 is mapped out; (d) reasonable geological/geochemical histories are described that lead to  
830 blueberry compositions consistent with the blueberry compositions associated with any of these  
831 groups; or, (e) it is rendered unlikely that any geological history could lead to the formation of  
832 blueberries with compositions consistent with the blueberry compositions associated with any  
833 group (and, hence, allow rejection of that group from further consideration). It is likely that the  
834 three groups already found are the only three. Demonstrating this soon is possible.

835 The APXS data on mixed-materials, basaltic soils, and dusty soils, as well as the  
836 homogeneity of the interiors of blueberries, the high quality composition data on Hawaiian  
837 blueberry analogs (Morris et al, 2005), the non-detection of silicates in blueberries (Calvin et al.,  
838 2009), and this analysis all point to blueberry compositions with hematite content of around 90  
839 wt% or, perhaps, 99+ wt%. Top loose blueberries are very plentiful (Calvin et al., 2009) and can  
840 be harvested (picked from the tops of smooth sheet and plains ripple soil bedforms) (Olsen,  
841 2021a) rather than mined (with blasting, drilling and digging). This means that top loose  
842 blueberries are an attractive source material for steel-making to produce sheet steel and steel  
843 powder to construct steel infrastructure for science on and around the Meridiani Planum.

844

845 **Appendix : Additional details on the selection of the data investigated**

846 The APXS data analyzed in this paper comes from *Opportunity*'s oxide abundance  
847 database stored in the file *apxs\_oxides\_mer1*.

848 This database file had records for 370 sample target composition distributions. Each  
849 record for a measured distribution included an identifier (ID), a classifying distribution type  
850 code, an unofficial name, the 16 measured oxide/element mass percentages for the distribution  
851 (although, for nickel, zinc and bromine these are given in derived mass percent in ppm), the 16  
852 errors on these measurements, and notes on the normalization constant and measurement  
853 integration time.

854

type	Soil Undisturbed (SU)	Soil Disturbed (SD)	Soil Trench (ST)	Soil Crest (SC)	Rock Undisturbed (RU)	Rock Brushed (RB)	Rock Ratted (RR)	Rock Ratted (RR1,RR2,RRB)	Cobble (C)	(CU)
number	36	18	4	0	193	55	46	9	0	9

855 Table A1. Numbers of database distributions by sample type.

856 The numbers of distributions by type in the database are given in Table A1. Only the two “berry  
857 bowl” measurements of the 212 measured distributions for rocks and cobbles are of interest to  
858 blueberry demixing, since for the main “berry bowl” measurement several blueberries were in  
859 the APXS's field of view (which was not the case for the other measured rock and cobble  
860 distributions). The two “berry bowl” distributions are not considered in this paper, but they may  
861 be analyzed in a future paper. The 18 disturbed soil and 4 trench soil distributions are of no  
862 interest to blueberry demixing. Soil crest distributions are now classified as undisturbed soils. All  
863 of the APXS distributions used here for demixing are now classified as undisturbed soils (SU),  
864 which has 36 sample distributions.

865 The blocked matrix presented in Figure 1 was blocked purely on the pairwise distance  
866 numbers and “blind” to the informal name annotation and without looking at MI photographs of  
867 the sample targets.

868 The two distributions in the minor block separating the two major blocks, *i.e.* B1974 and  
869 B237B, were each outliers to the two main blocks. The relatively short pairwise distances  
870 between the blueberry-mixture-like distribution B1974 and the distributions in the lower main  
871 block may be due to very high levels of dust sampled on sol 1974, since there was a thick layer  
872 of dust over the blueberries imaged by the MI on sol 1974 (see, for example,  
873 1M303431159E5BXP2976M2M1.JPG, but not reproduced here). No MI images were taken  
874 on sol 237, however all MI images for sol 238 (for example,  
875 1M149323195EFF35CRP2999M2M1.JPG) show a basaltic soil with a contact plate impression  
876 and this soil had unusually low levels of cohesion (it was sand-like) relative to other basaltic  
877 soils imaged.

878           The MI images (documenting sample-targets) associated with the 22 distributions in the  
879 largest of the matrix blocks in Figure 1 all showed blueberries, blueberry fragments or both, and  
880 most sols included images with contact plate impressions into the blueberry-containing mixtures.  
881 The MI images for four of the sample distributions (*i.e.* B369, B420B, B420 and B1647) were  
882 dominated by blueberry fragments in fragment ripples (indicated by a light-blue color in the  
883 vertical color-bar in Figure 1). The three distributions for the last three rows of the largest block  
884 in Figure 1 (*i.e.* B1145, B1148 and B023) all had relatively small numbers of blueberries in their  
885 associated MI sample target images. In contrast, the MI sample target images for distribution  
886 B1647 showed large numbers of large blueberry fragments. The Jensen-Shannon pairwise  
887 distances between distribution B1647 and the other distributions in the main block were  
888 relatively large. These large distances imply there is something noticeably different about the  
889 sample target for B1647, perhaps the target contained some chunks of Burns Formation  
890 sediment, the images of the sample target also showed thick layers of dust over the blueberry  
891 fragments. The distributions B1145, B1148 and B023 were not chosen for demixing due to their  
892 low blueberry content, while B1647 was not chosen because the sample mixture likely contained  
893 material beyond blueberries, blueberry fragments, basaltic soil and dust. Of the largest block's 18  
894 remaining distributions eight (*i.e.* B911, B091, B1140, B1755, B509, B100, B420, and B825)  
895 were not chosen for demixing since these distributions were all very similar to other  
896 distributions, and, hence, are considered alternate, redundant distributions. This leaves the  
897 following 10 mixed-material distributions that are chosen for demixing: B369, B910, B080,  
898 B420B, B505, B370, B2224, B443, B1136, and B416.

899           The 12 sample distributions in the second large block were ordered so that two major  
900 sub-blocks are apparent. Cross referencing with the archive of MI images shows that the  
901 distributions associated with the first sub-block (*i.e.* B3373, B730, B011, B249, B166, and  
902 B3925) were measured from basaltic soil targets with large grain sizes and only a thin dust layer,

903 while the MI images associated with the second sub-block distributions (*i.e.* B3925, B3836,  
904 B123, B060, B2957, and B3475) indicated that the sample targets had thick top-layers of light,  
905 fine-grained dust. Although, *Opportunity's* MI image archive associated with the relevant sols  
906 for this block was quite sparse - no MI images were taken on sols 730 and 3630, none again on  
907 sols 12 and 166 (although MI images of basaltic soils were taken on sols 12 and 167), no MI  
908 images were taken on sol 60 (but this is the "MontBlanc\_LesHauches" measurement that Morris  
909 et al. (2006) emphasize as a dusty soil target) while no contact plate impressions are seen in the  
910 MI images for sols 3925, 3836 and 2957. Five of the basaltic soil distributions (*i.e.*, B3373,  
911 B011, B249, B166, and B3630) and four of the dusty distributions (*i.e.*, B3836, B123, B060, and  
912 B3475) were chosen as filtering distributions in the demixing computations. The B730, B3925,  
913 and B2925 distributions were omitted because of a combination of redundancy with other  
914 distributions and a lack of MI photographic documentation of the sample targets. Although,  
915 B3925 later proved useful for defining the layer thickness of the outer layer of the space of dusty  
916 soil distributions.  
917

## 918 **Acknowledgments**

919 The sole author had no funding from any source, and has no financial conflict of interest.

## 920 **Open Research**

921 The APXS data used for searching mass-balance analysis in the study are available at the PDS  
922 Geosciences (GEO) Node and in the file `apxs_oxides_mer1.Opportunity.csv` via  
923 doi:10.17189/1518973 or <https://an.rsl.wustl.edu/merb/merxbrowser/an3.aspx> and is in the Public  
924 Domain (CCO).

925

926 The PanCam image data used for checking sampling locations are available at the PDS  
927 Geosciences (GEO) Node and NASA's *Opportunity* raw image archive at doi:10.17189/1518971 and  
928 <https://mars.nasa.gov/mer/gallery/all/opportunity.html> and is in the Public Domain (CCO).

929

930 The complete solution set data generated from the APXS data by the current research are available  
931 at the Zenodo Generalist Repository ([zenodo.org](https://zenodo.org)) via doi:10.5281/zenodo.5787305 with open  
932 access (a Creative Commons, CCO, license)

933

934

935 **References**

- 936 Arvidson, R. E., Poulet, F., Morris, R.V., Bibring, J.P., Bell III, J.F., Squyres, S.W., et al. (2006).  
937 Nature and origin of the hematite-bearing plains of Terra Meridiani based on analyses of orbital  
938 and Mars Exploration rover data sets. *Journal of Geophysical Research: Planets*, 111, E12S08.  
939 <https://doi.org/10.1029/2006JE002728>  
940
- 941 Bell, J. F., III, Squyres, S.W., Herkenhoff, K.E., Maki, J.N., Arneson, H.M., Brown, D., et al.  
942 (2003). Mars Exploration Rover Athena Panoramic Camera (PanCam) investigation. *Journal of*  
943 *Geophysical Research: Planets*, 108(E12), 8063. <https://doi.org/10.1029/2003JE002070>  
944
- 945 Bell, J. F., III, Squyres, S.W., Arvidson, R.E., Arneson, H.M., Bass, D., Calvin, W., et al. (2004).  
946 PanCam multispectral imaging results from the Opportunity Rover at Meridiani Planum.  
947 *Science*, 306 (5702), 1703–1709. <https://doi.org/10.1126/science.1105245>  
948
- 949 Braun, R., & Manning, R. M. (2007). Mars Exploration Entry, Descent, and Landing Challenges.  
950 *Journal of Spacecraft and Rockets*, 44(2), 310–328. <https://doi.org/10.2514/1.25116>  
951
- 952 Calvin, W. M., Shoffner, J. D., Johnson, J. R., Knoll, A. H., Pockock, J. M., Squyres, S. W., et al.  
953 (2009). Hematite spherules at Meridiani: Results from MI, Mini-TES, and PanCam. *Journal of*  
954 *Geophysical Research: Planets*, 113, E12S37. <https://doi.org/10.1029/2007JE003048>.  
955
- 956 Christensen, P. R., Bandfield, J.L., Clark, R.N., Edgett, K.S., Hamilton, V.E., Hoefen, T., et al.  
957 (2000). Detection of crystalline hematite mineralization on Mars by the Thermal Emission  
958 Spectrometer: Evidence for near-surface water. *Journal of Geophysical Research: Planets*, 105,  
959 9623–9642. <https://doi.org/10.1029/1999JE001093>  
960
- 961 Christensen, P. R., Mehall, G.L., Silverman, S.H., Anwar, S., Cannon, G., Gorelick, N., et al.  
962 (2003). Miniature Thermal Emission Spectrometer for the Mars Exploration Rovers. *Journal of*  
963 *Geophysical Research: Planets*, 108(E12), 8064. <https://doi.org/10.1029/2003JE002117>  
964
- 965 Christensen, P. R., & Ruff, S. W. (2004). Formation of the hematite-bearing unit in Meridiani  
966 Planum: Evidence for deposition in standing water. *Journal of Geophysical Research: Planets*,  
967 E08003. <https://doi.org/10.1029/2003JE002233>  
968
- 969 Christensen, P. R., Wyatt, M.B., Glotch, T.D., Rogers, A.D., Anwar, S., Arvidson, R.E., et al.  
970 (2004). Mineralogy at Meridiani Planum from the Mini-TES Experiment on the Opportunity  
971 Rover. *Science*, 306, (5702), 1733–1739. <https://doi.org/10.1126/science.1104909>  
972
- 973 Christensen, P. R., Ruff, S.W., Fergason, R., Gorelick, N., Jakosky, B.M., Lane, M.D., et al.  
974 (2005). Mars Exploration Rover candidate landing sites as viewed by THEMIS. *Icarus*, 176(1),  
975 12–43. <https://doi.org/10.1016/j.icarus.2005.01.004>  
976
- 977 Dunham, E. T., Balta, J. B., Wadhwa, M., Sharp, T. G., & McSween, H. Y. (2019). Petrology  
978 and geochemistry of olivine-phyric shergottites LAR 12095 and LAR 12240: Implications for  
979 their petrogenetic history on Mars. *Meteoritics & Planetary Science*, 54(4), 811–835.  
980 <https://doi.org/10.1111/maps.13262>

- 981  
982 Edgett, K. S. (1997). Nature and source of low-albedo surface material in the sandy aeolian  
983 environment of Sinus Meridiani, Mars. *Geology Society of America Abstract Programs*, 29,  
984 A214.
- 985  
986 Edgett, K. S., & Parker, T. J. (1997). Water on early Mars: Possible sub-aqueous sedimentary  
987 deposits covering ancient cratered terrain in western Arabia and Sinus Meridiani. *Geophysical*  
988 *Research Letters*, 24, 2897–2900. <https://doi.org/10.1029/97GL02840>
- 989  
990 Fenton, L. K., Michaels, T. I., & Chojnacki, M. (2015). Late Amazonian aeolian features,  
991 gradation, wind regimes, and Sediment State in the Vicinity of the Mars Exploration Rover  
992 Opportunity, Meridiani Planum, Mars. *Aeolian Research*, 16, 75–99.  
993 <https://doi.org/10.1016/j.aeolia.2014.11.004>
- 994  
995 Gellert, R., Rieder, R., Brückner, J., Clark, B. C., Dreibus, G., Klingelhöfer, G., et al. (2006).  
996 Alpha Particle X-Ray Spectrometer (APXS): Results from Gusev crater and calibration report.  
997 *Journal of Geophysical Research: Planets*, 111, E02S05. <https://doi.org/10.1029/2005JE002555>
- 998  
999 Gorevan, S., Myrick, T., Davis, K., Chau, J. J., Bartlett, P., Mukherjee, S., et al. (2003). Rock  
1000 Abrasion Tool Mars Exploration Rover Mission. *Journal of Geophysical Research: Planets*,  
1001 108(E12), 8068. <https://doi.org/10.1029/2003JE002061>
- 1002  
1003 Herkenhoff, K. E., Squyres, S. W., Bell, III, J.F., Maki, J. N., Arneson, H. M., Bertelsen, P., et  
1004 al. (2003). Athena Microscopic Imager investigation. *Journal of Geophysical Research: Planets*,  
1005 108(E12), 8065. <https://doi.org/10.1029/2003JE002076>
- 1006  
1007 Jolliff, B. L., & the Athena Science Team (2005). Composition of Meridiani hematite-rich  
1008 spherules: A mass-balance mixing model approach. In *Lunar Planetary Science, XXXVI*,  
1009 Abstract 2269.
- 1010  
1011 Jolliff, B. L., Clark, B. C., Mittlefehldt, D. W., Gellert, R., & the Athena Science Team (2007).  
1012 Compositions of Spherules and Rock Surfaces at Meridiani. In *Seventh International Conference*  
1013 *on Mars*, abstract 3374, Jet Propul. Lab., Pasadena, Calif.
- 1014  
1015 Jolliff, B. L., Gellert, R., & Mittlefehldt, D. W. (2007b). More on the possible composition of the  
1016 Meridiani hematite-rich concretions. In *Lunar Planetary Science, XXXVIII*, Abstract 2279.
- 1017  
1018 Klingelhöfer, G., Morris, R. V., Bernhardt, B., Rodionov, D., de Souza Jr, P. A., Squyres, S. W.,  
1019 et al. (2003). Athena MIMOS II Mössbauer spectrometer investigation. *Journal of Geophysical*  
1020 *Research: Planets*, 108 (E12), 8067. <https://doi.org/10.1029/2003JE002138>
- 1021  
1022 Klingelhöfer, G., Morris, R.V., Bernhardt, B., Schröder, C., Rodionov, D.S., de Souza Jr., P.A.,  
1023 et al. (2004). Jarosite and Hematite at Meridiani Planum from Opportunity's Mössbauer  
1024 Spectrometer. *Science*, 306 (5702), 1740–1745. <https://doi.org/10.1126/science.1104653>
- 1025  
1026 Mars Exploration Rover APXS Team. (2016). MER APXS Derived Oxide Data Bundle. PDS  
1027 Geosciences (GEO) Node. <https://doi.org/10.17189/1518973>

1028

1029 Mars Exploration Rover Microscopic Imager Team (2016). MER1 Microscopic Imager Science  
1030 Raw Data Bundle. PDS Geosciences (GEO) Node. <https://doi.org/10.17189/1518971>

1031

1032 Morris, R. V., Golden, D. C., Bell III, J. F., Shelfer, T. D., Scheinost, A. C., Hinman, N. W., et  
1033 al. (2000). Mineralogy, composition, and alteration of Mars Pathfinder rocks and soils: Evidence  
1034 from multispectral, elemental, and magnetic data on terrestrial analogue, SNC meteorite, and  
1035 Pathfinder samples. *Journal of Geophysical Research: Planets*, 105, 1757–1817.  
1036 <https://doi.org/10.1029/1999JE001059>

1037

1038 Morris, R.V., Ming, D. W., Graff, T. G., Arvidson, R. E., Bell III, J. F., Squyres, S. W., et al.  
1039 (2005). Hematite spherules in basaltic tephra altered under aqueous, acid-sulfate conditions on  
1040 Mauna Kea volcano, Hawaii: Possible clues for the occurrence of hematite-rich spherules in the  
1041 Burns formation at Meridiani Planum, Mars. *Earth and Planetary Science Letters*, 240, 168–  
1042 178. <https://doi.org/10.1016/j.epsl.2005.09.044>

1043

1044 Morris, R. V., Klingelhöfer, G., Schröder, C., Rodionov, D.S., Yen, A., Ming, D.W., et al.  
1045 (2006). Mössbauer mineralogy of rock, soil, and dust at Meridiani Planum, Mars: Opportunity's  
1046 journey across sulfate-rich outcrop, basaltic sand and dust, and hematite lag deposits. *Journal of*  
1047 *Geophysical Research: Planets*, 111(E12S15), 8068. <https://doi.org/10.1029/2006JE002791>

1048

1049 Olsen, R. M. (2021a). Iron Oxide Harvesting on Mars. In *AIAA ASCEND 2021*, 4037, Las  
1050 Vegas, Nevada & Virtual. <https://doi.org/10.2514/6.2021-4037>

1051

1052 Olsen, R. M. (2021b). Searching Mass-Balance Analysis to Find the Composition of Martian  
1053 Blueberries: Database of Complete Solution Sets. Zenodo.  
1054 <https://doi.org/10.5281/zenodo.5787305>

1055

1056 Pang, K-N, Li, C., Zhou, M-F., & Ripley, E.M. (2008). Abundant Fe–Ti oxide inclusions in  
1057 olivine from the Panzhihua and Hongge layered intrusions, SW China: evidence for early  
1058 saturation of Fe–Ti oxides in ferrobaltic magma. *Contributions to Mineralogy and Petrology*,  
1059 158, 307-321. <https://doi.org/10.1007/s00410-008-0287-z>

1060

1061 Rieder, R., Gellert, R., Brückner, J., Klingelhöfer, G., Dreibus, G., Yen, A., & Squyres, S.W.  
1062 (2003). The new Athena alpha particle X-ray spectrometer for the Mars Exploration Rovers.  
1063 *Journal of Geophysical Research: Planets*, 108 (E12), 8066.  
1064 <https://doi.org/10.1029/2003JE002150>

1065

1066 Rieder, R., Gellert, R., Anderson, R.C., Brückner, J., Clark, B.C., Dreibus, G., et al. (2004).  
1067 Chemistry of Rocks and Soils at Meridiani Planum from the Alpha Particle X-ray Spectrometer.  
1068 *Science*, 306 (5702), 1746–1749. <https://doi.org/10.1126/science.1104358>

1069

1070 Soderblom, L. A., Anderson, R.C., Arvidson, R.E., Bell III, J.F., Cabrol, N.A., Calvin, W., et al.  
1071 (2004). Soils of Eagle Crater and Meridiani Planum at the Opportunity Rover Landing Site.  
1072 *Science*, 306(5702), 1723–1726. <https://doi.org/10.1126/science.1105127>

1073

- 1074 Squyres, S. W., Arvidson, R. E., Baumgartner, E. T., Bell III, J. F., Christensen, P. R., Gorevan,  
1075 S., et al. (2003). Athena Mars Rover science investigation. *Journal of Geophysical Research:*  
1076 *Planets*, 108 (E12), 8062. <https://doi.org/10.1029/2003JE002121>  
1077
- 1078 Squyres, S. W., Grotzinger, J.P., Arvidson, R.E., Bell III, J.F., Calvin, W., Christensen, P.R., et  
1079 al. (2004). In Situ Evidence for an Ancient Aqueous Environment at Meridiani Planum, Mars.  
1080 *Science*, 306 (5702), 1709–1714. <https://doi.org/10.1126/science.1104559>  
1081
- 1082 Tirsch, D., Craddock, R.A., Platz, T., Maturilli, A., Helbert, J., & Jaumann, R. (2012). Spectral  
1083 and petrologic analyses of basaltic sands in Ka’u Desert (Hawaii) – implications for the dark  
1084 dunes on Mars. *Earth Surface Processes and Landforms*, 37, 434–448.  
1085 <https://doi.org/10.1002/esp.2266>  
1086